Acta Pharmaceutica Sinica B 2025;15(3):1626−1642

Chinese Pharmaceutical Association
Institute of Materia Medica, Chinese Academy of Medical Sciences

Acta Pharmaceutica Sinica B

www.elsevier.com/locate/apsb
www.sciencedirect.com

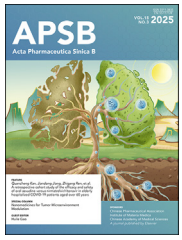

ORIGINAL ARTICLE

Optineurin restrains CCR7 degradation to guide type II collagen-stimulated dendritic cell migration in rheumatoid arthritis

Wenxiang Hong[a,b], Hongbo Ma[a], Zhaoxu Yang[a], Jiaying Wang[a,c], Bowen Peng[a], Longling Wang[a], Yiwen Du[a], Lijun Yang[a,d], Lijiang Zhang[d], Zhibin Li[a,e], Han Huang[a], Difeng Zhu[a], Bo Yang[a,f], Qiaojun He[a,c], Jiajia Wang[a,b,*], Qinjie Weng[a,b,c,g,*]

[a]*Center for Drug Safety Evaluation and Research, Zhejiang Province Key Laboratory of Anti-Cancer Drug Research, College of Pharmaceutical Sciences, Zhejiang University, Hangzhou 310058, China*
[b]*Nanhu Brain-Computer Interface Institute, Hangzhou 311100, China*
[c]*The Second Affiliated Hospital, Zhejiang University School of Medicine, Hangzhou 310009, China*
[d]*Key Laboratory of Drug Safety Evaluation and Research of Zhejiang Province, Center of Safety Evaluation and Research, Hangzhou Medical College, Hangzhou 310059, China*
[e]*Hangzhou Institute of Innovative Medicine, Zhejiang University, Hangzhou 310018, China*
[f]*School of Medicine, Hangzhou City University, Hangzhou 310015, China*
[g]*Taizhou Institute of Zhejiang University, Taizhou 318000, China*

Received 7 May 2024; received in revised form 28 July 2024; accepted 19 December 2024

KEY WORDS

Rheumatoid arthritis;
Dendritic cells;
Migration;
Optineurin;
CCR7;
Degradation;
Saikosaponin D;
Type II collagen

Abstract Dendritic cells (DCs) serve as the primary antigen-presenting cells in autoimmune diseases, like rheumatoid arthritis (RA), and exhibit distinct signaling profiles due to antigenic diversity. Type II collagen (CII) has been recognized as an RA-specific antigen; however, little is known about CII-stimulated DCs, limiting the development of RA-specific therapeutic interventions. In this study, we show that CII-stimulated DCs display a preferential gene expression profile associated with migration, offering a new perspective for targeting DC migration in RA treatment. Then, saikosaponin D (SSD) was identified as a compound capable of blocking CII-induced DC migration and effectively ameliorating arthritis. Optineurin (OPTN) is further revealed as a potential SSD target, with *Optn* deletion impairing CII-pulsed DC migration without affecting maturation. Function analyses uncover that OPTN prevents the proteasomal transport and ubiquitin-dependent degradation of C−C chemokine receptor 7 (CCR7), a pivotal

*Corresponding authors.
E-mail addresses: wengqinjie@zju.edu.cn (Qinjie Weng), wangjiajia3301@zju.edu.cn (Jiajia Wang).

Peer review under the responsibility of Chinese Pharmaceutical Association and Institute of Materia Medica, Chinese Academy of Medical Sciences.

https://doi.org/10.1016/j.apsb.2025.02.004

chemokine receptor in DC migration. *Optn*-deficient DCs exhibit reduced CCR7 expression, leading to slower migration in CII-surrounded environment, thus alleviating arthritis progression. Our findings underscore the significance of antigen-specific DC activation in RA and suggest OPTN is a crucial regulator of CII-specific DC migration. OPTN emerges as a promising drug target for RA, potentially offering significant value for the therapeutic management of RA.

1. Introduction

Dendritic cells (DCs) are the most potent professional antigen-presenting cells, acting as a crucial link in maintaining tissue tolerance to harmless environmental antigens or in initiating adaptive immunity against pathogens. Once stimulated by "danger signals", immature DCs rapidly migrate to peripheral tissues to capture antigens, where they can be converted into mature DCs and up-regulate the expression of C−C chemokine receptor 7 (CCR7) upon antigen uptake[1-3]. Subsequently, antigen-carrying mature DCs are guided by the CCR7 ligands CCL19 and CCL21 to traffic to lymph nodes, where they present the acquired antigens to naïve T cells, thereby eliciting adaptive immunity[4,5]. Thus, re-infusion of tolerogenic DCs mitigates symptoms in autoimmune diseases such as rheumatoid arthritis (RA), a systemic, chronic, and progressive condition that characteristically affects peripheral joints with synovial inflammation, swelling, and bone destruction[6-9]. Strategies that interfere with DC migration, including gene modification, pharmaceutical interventions, or vaccination, represent a promising and valuable approach to treating autoimmune diseases[4,10,11]. In total, DCs play a central role in the disruption of immune homeostasis during the onset and progression of autoimmune diseases[5,12].

Autoimmune diseases arise when the immune system mounts a specific response against self-antigens. Typically, it is impossible for immune effectors to completely eliminate these antigens, resulting in a sustained immune response that leads to chronic inflammatory damage to tissues[13-15]. Despite their significance, pinpointing the self-antigens implicated in autoimmune diseases remains challenging. RA is characterized by synovial inflammation and cartilage destruction, type II collagen (CII), normally sequestered within the intact articular cartilage, has been recognized as a pertinent joint-specific self-antigen[16-18]. An increased release of CII has been observed in RA patients, which aggrandizes the exposure of this self-antigen to DCs in the synovium[13,19]. Subsequently, mature DCs will further induce cartilage degradation upon exposure to CII, thus establishing a positive feedback loop that amplifies inflammation[13,20]. Moreover, the transfer of collagen-pulsed DCs into congenic recipient mice is sufficient to spontaneously induce arthritis, underscoring the critical role of DCs and disease-specific CII antigens in RA development[7,21].

Emerging evidence suggests that DC activation is significantly influenced by the complex antigenic microenvironment, which leads to distinct signaling profiles within DCs upon various antigen stimulation[21,22]. It has been reported that treatment with anti-OSCAR mAb completely inhibits CII-induced DC activation but does not affect cytokine release stimulated by lipopolysaccharide (LPS)[22]. Analogously, knockout of *Tarm1* has been shown to suppress DC maturation in response to CII challenge, while not affecting maturation induced by other stimuli like LPS, cytosine-phosphate-guanine (CpG), and polyinosinic-polycytidylic acid (PolyI:C)[23]. Nonetheless, our understanding of the comprehensive changes in DC signaling or function following CII stimulation remains limited, which constrains the identification of disease-specific drug targets and the development of effective therapeutic agents.

Optineurin (OPTN), initially identified as a binding partner for adenoviral protein, is implicated in numerous biological processes, including autophagy, vesicle trafficking and receptor regulation[24-27]. Genetic variations, such as mutations or polymorphisms, in the *OPTN* gene have been associated with a spectrum of disorders like primary open-angle glaucoma, amyotrophic lateral sclerosis, Paget's disease of the bone, and Crohn's disease, all of which exhibit links to immune system dysregulation[25,26,28,29]. Certain pro-inflammatory cytokines, exemplified by interferon-gamma (IFNγ), have been shown to upregulate OPTN expression[30]. Notably, our previous work has revealed that depletion of *Optn* in DCs facilitates the establishment of an IL10/janus kinase 2 (JAK2)/signal transducer and activator of transcription 3 (STAT3)/IL10 positive feedback loop, which in turn hampers DC maturation and curbs the progression of experimental autoimmune encephalitis, thereby highlighting the involvement of OPTN in DC functionality and autoimmunity[31]. Additionally, a recent study has indicated that OPTN can inhibit the expression of the receptor activator of nuclear factor kappa-B (NF-κB) ligand in synovial fibroblasts *in vitro*, thus impeding osteoclast differentiation[32]. However, the role of OPTN in RA-specific DCs by CII stimulation remains to be elucidated.

Herein, we showed that CII induces a distinct gene profile in DCs, potently promoting their migration and offering novel insights for RA treatment. Natural compounds, with their extensive biological activities and favorable safety profiles, hold significant therapeutic potential for autoimmune diseases[33-37]. Saikosaponin D (SSD), a triterpene saponin derived from Bupleuri Radix, exhibits a variety of pharmaceutical properties, including anti-fibrosis, anti-inflammatory, immunomodulatory, anti-depressant, and anti-tumor effects[38-40]. Through screening of natural compound databases, SSD was identified to interdict CII-induced DC migration and relieve arthritis, potentially through targeting OPTN. Gain and loss of function studies revealed OPTN sustains CCR7 protein homeostasis by inhibiting its proteasomal degradation, thus promoting DC migration and the progression of RA. Our findings underscore the importance of modulating disease- or antigen-specific DC activation and demonstrate the therapeutic efficacy of targeting OPTN in RA.

2. Materials and methods

2.1. Mice

DBA/1J mice were purchased from Shanghai Slac Laboratory Animal Co., Ltd. *CD11c*-Cre mice were obtained from the Jackson Laboratory. *Optn* KO and *Optn*$^{flox/flox}$ mice were gifted by Prof. Ronggui Hu (Zhejiang University School of Medicine, Hangzhou, China). The CD11c^{+} dendritic cells conditional *Optn* knockout mice (*Optn* cKO mice) were generated by breeding *Optn*$^{flox/flox}$ with *CD11c*-Cre transgenic mice. All mice were supplied with standard laboratory diet and water ad libitum and housed in specific pathogen-free environment at 20 ± 2 °C and 65 ± 5% humidity, with a 12-h light/dark cycle. All animal experiments were approved by the Institutional Animal Care and Use Committee (IACUC) at Zhejiang University (IACUC-s21-017) and performed in compliance with all relevant ethical regulations.

2.2. Induction and assessment of CIA

CIA mouse model was induced as described previously[23,41-43]. In brief, male 8-week-old DBA/1J mice were immunized subcutaneously at the base of the tail and thigh with 200 μg immunization grade chick type II collagen (CII, 20011, 2 mg/mL, Chondrex, WA, USA) emulsified 1:1 in Freund's adjuvant, complete (F5881, Sigma, MI, USA) containing 5 mg/mL *Mycobacterium tuberculosis* H37Ra (231141, BD Difco, NJ, USA) on Day 0, and boosted by the injection of another 200 μg CII (emulsified with incomplete freund's adjuvant) near the primary injection site on Day 21.

All mice were subsequently monitored for signs of arthritis through visual scoring and foot thickness measurement every 3 days from Day 24 and finally sacrificed on Day 45 for evaluation. Every paw will receive a CIA score from 0 to 4, and the maximum CIA score can reach 16 as follows: score 0, healthy; score 1, mild redness and swelling of tarsal joints or limited to individual digits; score 2, moderate erythema and swelling extending to digits or ankle; score 3, serious redness and swelling of the entire paw; score 4, ankylosis of the limb with involvement of multiple joints[23,43,44].

2.3. Histological staining

Hind limbs collected from CIA mice were fixed in 10% formalin for at least 48 h followed by decalcifying with 5% formic acid, dehydrating and paraffin embedding. Then 5-μm thick sections were deparaffinized and stained with H&E or alcian. Synovitis, pannus and bone erosion were scored on a scale of 0−4 as follows: score 0, healthy and no signs of inflammation; score 1, mild inflammation with the hyperplasia of the synovial lining; score 2, granulomatous lesions in the synovial sublining tissue; score 3, pannus formation and cartilage destruction; score 4, severe inflammatory cell infiltrate and disappearance of bone structure[23,42,44]. Articular cartilage areas indicated by alcian staining were quantified by Image J software.

2.4. Elisa for CII-specific serum IgG

The level of anti-CII IgG in serum was measured by ELISA according to the manufacturer's protocols. In brief, the ELISA plate (3590, Solarbio, Beijing, China) is coated with 50 μg/mL CII overnight at 4 °C and then blocked with 4% bovine serum albumin at room temperature for 1 h. After incubating with different serum samples for 2 h and followed by goat anti-mouse IgG/HRP (SE131, Solarbio) for 2 h at 37 °C, ELISA plate is colored by TMB solution and detected in 450 nm.

2.5. Cell culture

For BMDC isolation and culture, bone marrow from 6−8-week-old mice was resuspended and cultured in RPMI-1640 (Gibco, New York, USA) medium supplemented with 10% fetal bovine serum (Gibco), 100 mg/mL penicillin, 100 mg/mL streptomycin, 50 ng/mL recombinant murine GM-CSF (315-03, Peprotech, NJ, USA), and 20 ng/mL recombinant murine IL-4 (214-14, Peprotech). Half medium was replaced by fresh medium every 3 days.

DC2.4 cell line, which was gifted by Prof. Zhen Gu (Zhejiang University, Hangzhou, China), was cultured in RPMI-1640 containing 10% fetal bovine serum, 100 mg/mL penicillin, and 100 mg/mL streptomycin. Cells were maintained in a humidified atmosphere containing 5% CO_2 at 37 °C.

2.6. Chemical treatment

In CIA mouse model, saikosaponian D (SSD, B20150, 20 mg/kg, dissolved in 5% DMSO + 95% saline solution, Shanghai yuanye Bio-Technology, Shanghai, China) or solvent control was given by i.g. daily from Day 21.

For BMDC or DC2.4, cells were treated with 50 ng/mL lipopolysaccharides (LPS, L118716, Aladdin, USA) for the indicated time, 100 μg/mL CII for the indicated time, 1 μmol/L SSD for 24 h, 20 μg/mL cycloheximide (HY-12320, MCE, NJ, USA) for the indicated time, 10 μmol/L MG-132 (T2154, TargetMol, Shanghai, China) for 12 h, 10 μmol/L chloroquine (C6628, Sigma) for 12 h, 10 μmol/L bafilomycin (T6740, TargetMol) for 12 h, 10 μmol/L rapamycin (T1537, TargetMol) for 12 h.

2.7. In vitro transwell assay for DC migration

The *in vitro* Transwell assay was performed by 24-well plates together with 8 μm pore size Transparent PET Membrane (353097, Falcon, NJ, USA). 600 μL culture medium containing 50 ng/mL recombinant mouse CCL19 (587806, BioLegend, CA, USA) and recombinant mouse CCL21 (586402, BioLegend) was added to the lower chamber. BMDCs or DC2.4 (5×10^4 cells in a total volume of 200 μL culture medium) were added to the upper chamber. After 12 h, the number of BMDCs that migrated to the lower chamber was determined by cell counter or flow cytometry, while migrated DC2.4 were visualized by crystal violet staining and microphotography.

2.8. In vivo assay for DC migration

BMDCs were labeled with 5 μmol/L CFSE cell division tracker kit (423801, BioLegend) according to the manufacturer's protocols. Then, 5×10^6 CSFE-labeled BMDCs were injected in the hind leg footpad of recipient mice subcutaneously, and the percentage of CFSE^{+} cells in lymph nodes was evaluated by flow cytometry after 48 h injection.

2.9. Flow cytometry

For cell surface staining, single cell suspensions were incubated for 30 min at 4 °C with PE anti-mouse CD11c antibody (117308, BioLegend), FITC anti-mouse CD80 antibody (104706, BioLegend), PE/Cyanine7 anti-mouse CD86 antibody (105014,

BioLegend), PerCP/Cyanine5.5 anti-mouse I-A/I-E antibody (107626, BioLegend), APC anti-mouse CD197 (CCR7) antibody (120107, BioLegend). For intracellular staining of cytokines, single cell suspensions from DLN of the indicated mice were stained with FITC rat anti-mouse CD4 (553047, BD Biosciences, CA, USA) for 30 min at 4 °C, followed by staining with PE rat anti-mouse IFN-γ (554412, BD Biosciences) and PE anti-mouse IL-17A antibody (506904, Biolegend) for 30 min at 4 °C using Cytofix/Cytoperm kit (00-5523-00, ThermoFisher, MA, USA) according to the manufacturer's instructions. Samples were washed and then analyzed by FACS versus flow cytometry (ACEA NovoCyte or BD Biosciences, USA).

2.10. Western blotting

Cells were washed with PBS and then lysed in lysis buffer (0.2% Triton X-100, 0.3% NP-40, 0.1% PMSF, 0.1% $NaVO_3$, and 0.25% Leupeptin). Protein extracts were separated by SDS-PAGE (8%−12%) and blotted to PVDF membranes. After blocking with 5% fat-free milk at room temperature for 1 h, different strips were incubated with the following primary antibodies at 4 °C overnight: COX-2 antibody (M-19) (sc-1747, Santa Cruz Biotechnology, TX, USA), CDK2 antibody (D-12) (sc-6248, Santa Cruz Biotechnology), optineurin antibody (C-2) (sc-166576, Santa Cruz Biotechnology), anti-optineurin antibody (ab23666, Abcam, Cambridge, Britain), phospho-STAT3 (Tyr705) (D3A7) XP® rabbit mAb (#9145, Cell Signaling Technology, MA, USA), STAT3 (124H6) mouse mAb (#9139, Cell Signaling Technology), phospho-JAK2 (Tyr1007/1008) antibody (#3771, Cell Signaling Technology), JAK2 (D2E12) XP® rabbit mAb (#3230, Cell Signaling Technology), TBK1/NAK antibody (#3013, Cell Signaling Technology), CCR7 recombinant rabbit monoclonal antibody (ET1602-22, Huabio, Hangzhou, China), CCR2 recombinant rabbit monoclonal antibody (ET1611-65, Huabio), anti-CXCR4 antibody (ab124824, Abcam), HA-Tag (C29F4) rabbit mAb (#3724, Cell Signaling Technology), ubiquitin antibody (P4D1) (sc-8017, Santa Cruz Biotechnology), anti-SQSTM1/p62 antibody (ab56416, Abcam), LC3A/B (D3U4C) XP® Rabbit mAb (#12741, Cell Signaling Technology), GAPDH rabbit pAb (db106, DiagBio Technology, Hangzhou, China). The membranes were further stained by secondary horseradish peroxidase-conjugated IgG at room temperature for 1 h and visualized with NcmECL high (P2100, NCM Biotech, Suzhou, China). Images were finally taken by GE AI100 or azure biosystem.

2.11. RNA isolation and quantitative real-time PCR assays

Total RNA was isolated from cells with RNAiso Plus (9109, Takara, Shiga, Japan), and cDNA was then transcribed using TransScript One-Step gDNA Removal and cDNA Synthesis SuperMix (AT311-03, TransGen Biotech, Beijing, China) according to the manufacturer's protocols. qRT-PCR analysis was then performed using Taq pro universal SYBR qPCR master mix (Q712-02, Vazyme, Nanjing, China) method on QuantStudio 6 Flex Real-Time PCR System (Applied Biosystems, Carlsbad, CA, USA). The gene expression was normalized to *Gapdh* and quantified by the $2^{-\Delta\Delta CT}$ method. Sequences of the primers for qRT-PCR are shown in Supporting Information Table S1.

2.12. Immunofluorescence

DC2.4 cells were washed by PBS and then fixed with 4% PFA for 20 min at 4 °C, followed by the permeabilization in 0.3% Triton X-100 for 5 min and the incubation with blocking buffer for 15 min at room temperature. Cells were then stained with 20S proteasome α2 antibody (B-4) (sc-377148, Santa Cruz Biotechnology) or ubiquitin antibody (P4D1) (sc-8017, Santa Cruz Biotechnology) overnight at 4 °C. Subsequently, washed cells were incubated with Alexa Fluor 568-coupled secondary antibodies (A10037, Life Technologies, CA, USA) and DAPI (D212, Dojindo, Kumamoto, Japan) for 45 min at room temperature. For F-Actin staining, BMDCs were washed by PBS and then fixed with 4% PFA, followed by staining with anti-MHC class II antibody (ab139365, Abcam) for 1 h and Alexa Fluor 568-coupled secondary antibodies (A78946, Life Technologies) for 45 min at room temperature. Subsequently, washed cells were permeabilized by 0.3% Triton X-100 for 5 min and incubated with Actin-Tracker Green-488 (C2201S, Beyotime, Shanghai, China) by the manufacturer's procedure and counterstained with DAPI. Images were captured by TCS SP8 confocal (Leica, Wetzlar, Germany).

2.13. Co-immunoprecipitation

For co-immunoprecipitation of exogenous protein, transfected DC2.4 were lysed in lysis buffer supplemented with a protease inhibitor cocktail as described. Whole-cell lysates were incubated with anti-DYKDDDDK G1 affinity resin (L00432, GenScript, Nanjing, China) or anti-HA magnetic beads (B26201, Selleck Chemicals, TX, USA) at 4 °C overnight. For co-immunoprecipitation of endogenous protein, whole-cell lysates of BMDCs were incubated with CCR7 recombinant rabbit monoclonal antibody (ET1602-22, Huabio) or control IgG coupled to protein A/G magnetic beads (B23201, Bimake, TX, USA) at 4 °C overnight. Then, samples were washed by wash buffer at least eight times, and boiled in SDS loading buffer. Immunoprecipitated protein complexes were detected using Western blotting.

2.14. Plasmid and siRNA transfection

Following the manufacturer's protocols, transient transfection was performed using jet medium and jetPRIME (114-15, Polyplus, Strasbourg, France) in 6-well plates with 1 μg of indicated plasmid or 2.5 μL of indicated siRNA. The siRNAs of mouse *Optn* (5′-GAAGTCACAAAGAGGAATCTA-3′) were synthesized by GenePharma (Suzhou, China).

2.15. RNA sequencing and data analysis

Total RNA was extracted from CII-challenged WT and *Optn* KO BMDCs according to manufacturer's instructions, and then subjected to cDNA library construction and RNA sequencing (Novogene, Beijing, China). Cuff-diff was used to estimate fragments per kilobase of transcript per million mapped reads (FPKM) values for known transcripts and to analyze differentially expressed transcripts. In all differential expression tests, a difference was considered significant when $P < 0.05$, fold change >1.5.

The volcano plot was plotted according to https://www.omicstudio.cn/tool. The heatmap of gene expression was generated using the R language (version 4.3.0). Gene ontology analysis of gene expression changes was performed using ToppGene Suite (https://toppgene.cchmc.org/) and Gene Set Enrichment Analysis (GSEA_4.3.2; http://www.broadinstitute.org/gsea/index.jsp). Normalized enrichment score (NES) reflects the degree to which the gene set is overrepresented at the top or bottom of a ranked list of genes.

2.16. *Affymetrix microarray gene chip and gene tree analysis*

Differential gene expression was analyzed by "Limma" (v3.46.0) package for R (v4.0.4) (https://www.r-project.org/). Genes with P value < 0.05 and absolute $Log_2FC > 1$ were identified as differentially expressed genes. The function of "cutree_rows" in the "pheatmap" (v1.0.12) package was used to cluster the gene expression patterns. The cell migration-related genes were selected based on the ToppGene Suite (https://toppgene.cchmc.org/enrichment.jsp), and gene tree analysis about these genes' expression in different samples was then calculated and visualized by "ggplot2" (v3.3.5) packages.

2.17. *Acquisition of RA- and SSD-associated targets*

GeneCards (http://www.genecards.org/) database was used for the prediction of signals associated with rheumatoid arthritis. In addition, Herb (http://herb.ac.cn/), SwissTargetPrediction (http://www.swisstargetprediction.ch/), STITCH (http://stitch.embl.de), PharmMapper (http://lilab-ecust.cn) and Pubmed (https://pubmed.ncbi.nlm.nih.gov/) databases were used to obtain the potential targets of SSD.

2.18. *Statistical analysis*

Statistical comparisons were performed using GraphPad Prism software (version 8.0.1). Unpaired two-tailed Student's t-test was performed to assess the statistical significance between two groups, while one-way ANOVA Tukey's *post hoc* analysis was used for multiple comparisons. All data were from at least three independent experiments and presented as mean ± standard deviation (SD). P value < 0.05 was considered statistically significant (represented as $*P < 0.05$, $**P < 0.01$, $***P < 0.001$, or not significant (ns)).

3. Results

3.1. *RA specific antigen CII prefers to activate DC migration signaling*

Considering the specific antigen uptake, processing, and presentation capabilities of DCs with distinct signaling activation, along with their pivotal role in the development of RA, human peripheral blood monocyte-derived DCs were exposed to CII (a specific antigen for RA) or LPS (a common DC activator) for 20 h[22]. Subsequently, RNA was extracted and subjected to high-throughput analysis (Fig. 1A). Differentially expressed genes (fold change >2, $P < 0.05$) were identified in CII and LPS-challenged DCs when compared with the control group (Fig. 1B). As depicted in Fig. 1C−E, upregulated genes were extracted to elucidate the signaling pathways preferentially activated in CII-challenged DCs. Notably, DC maturation-associated enrichment was found in 489 genes that exclusively upregulated in LPS-treated DCs (Cluster 1), indicating DC maturation-related genes are not unique to CII-stimulated DCs. Interestingly, CII specifically upregulated the expression of 87 genes (Cluster 3), including *CXCL5*, *MMP3*, and *GREM1*, which were enriched in leukocyte chemotaxis, regulation of cell migration, positive regulation of cell motility, and cell adhesion (Fig. 1C−E). Besides, Gene tree analysis showed that CII, but not LPS, significantly enhanced the expression of human DC migration-related genes (Fig. 1F). This finding was corroborated by qRT-PCR in both murine bone marrow-derived dendritic cells (BMDCs) and mouse dendritic cell line DC2.4 (Supporting Information Fig. S1A and S1B).

Interestingly, the 273 genes that were co-upregulated in Cluster 2 were also found to be enriched in positive regulation of cell migration (Fig. 1D and E), suggesting LPS is also able to induce DC migration. However, gene set enrichment analysis (GSEA) revealed that gene signatures associated with cell migration regulation, including selective expression of chemokine receptors, focal adhesion, and actin filament bundle organization, were more prominently enriched in DCs stimulated by CII compared to those stimulated by LPS (Fig. 1G and H). Hence, we conducted an *in vitro* Transwell assay to evaluate the migration of antigen-stimulated mature BMDCs in response to CCL19 and CCL21, two ligands for the key mature DC migration signaling receptor CCR7[45]. Results showed that CII induced a stronger migration response in BMDCs than LPS (Fig. 1I). Therefore, we concluded that CII has a preferential effect on activating DC migration signaling pathways, which has implications for targeting DC migration in response to CII antigenic stimuli.

On the other hand, we also examined the down-regulated genes following LPS or CII stimulation. A Venn diagram revealed that 689 genes that exclusively down-regulated after LPS stimulation were enriched in gene signatures associated with mitochondria, while 74 genes that solely reduced in CII-induced DCs were enriched in gene signatures related to ubiquitin protein ligase activity (Fig. S1C and S1D). These findings may hold significance for further investigation.

3.2. *SSD is screened with the suppression of CII-induced DC migration*

Since the multiple therapeutic roles with low toxicity profile of natural resources, we then explored the possible natural monomers that may alleviate RA *via* inhibiting DC migration in multifarious databases (Supporting Information Fig. S2). First, several herbs, like Radix Bupleuri, were extracted to be related to "Rheumatoid arthritis treatment" in the Traditional Chinese Medicine Systems Pharmacology Database and Analysis Platform (TCMSP). Then, to obtain the ideal active components with great pharmacokinetic information[46-48], the potential pharmaceutical ingredients of Radix Bupleuri were further filtered by several parameters like oral bioavailability (>30%) and Lipid/water Partition Coeffici (Alog$P$, >0 and <3). According to the regulatory signal analysis of these ingredients in the HERB database, we paid attention to SSD, one main active ingredient of Radix Bupleuri, because the differentially expressed genes regulated by SSD were enriched in the gene signatures associated with cell migration (Fig. S2).

Results showed that SSD treatment significantly inhibited CII-induced BMDC migration from the upper chamber to the lower chamber, and the number of migrated cells decreased from 41417 ± 9257 to 10250 ± 4293 (Fig. 2A and B). In addition, control and SSD-pretreated BMDCs were labeled with carboxyfluorescein diacetate succinimidyl ester (CFSE) and then injected into the hind footpad of mice (Fig. 2C), flow cytometry results of the migrated $CFSE^+$ BMDCs in draining lymph node (DLN) suggested SSD pretreatment impeded $CFSE^+$ BMDC migration *in vivo* (Fig. 2D). Thus, these data indicate a strong suppression of SSD on CII-induced DC migration.

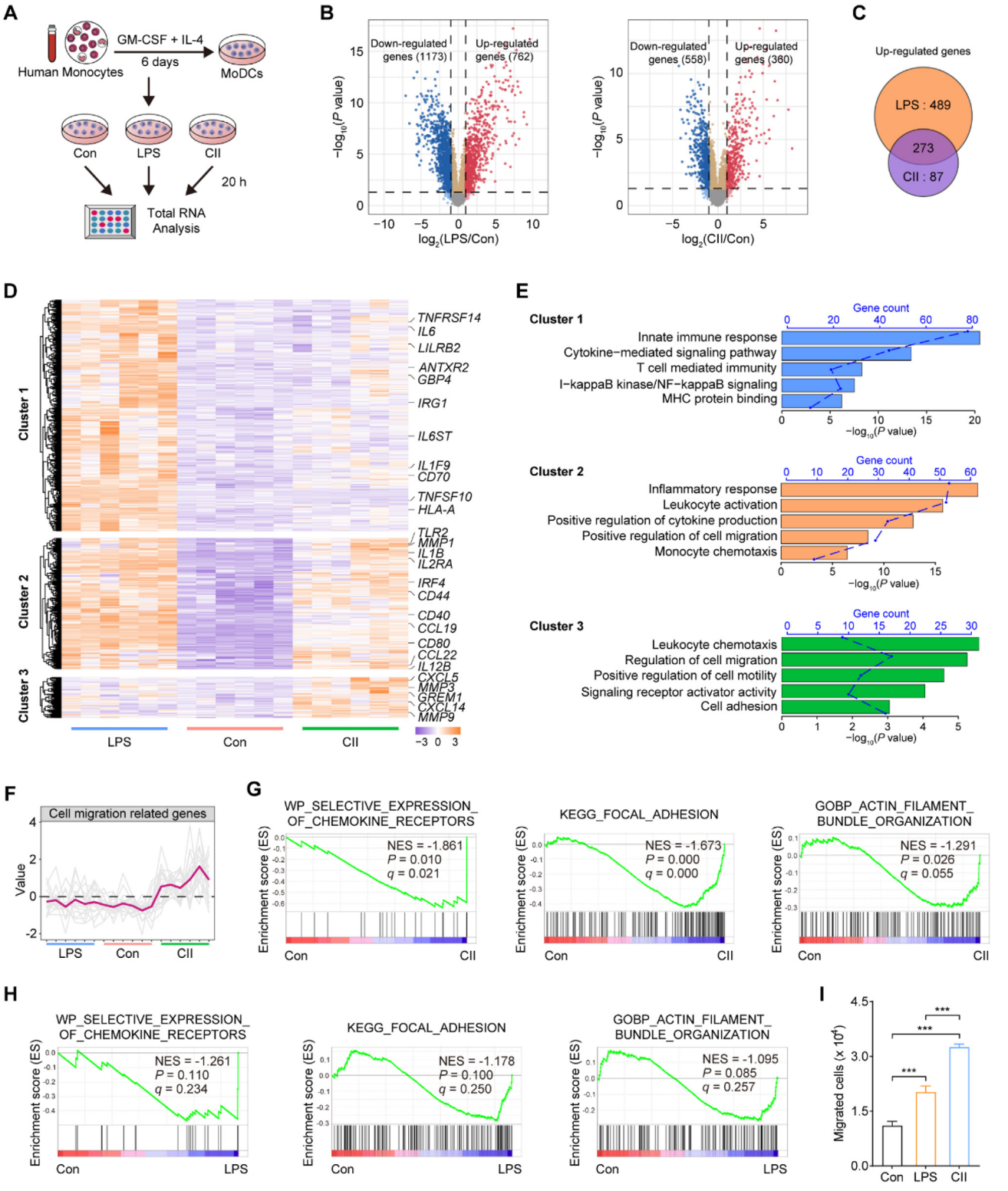

Figure 1 CII establishes a characteristic gene profile to activate DC migration. (A) Scheme of the experimental approach for Affymetrix microarray gene chip analysis from the EMBL-EBI database (accession no. E-MTAB-2904). (B) Volcano plot of genes differentially expressed in human MoDCs after LPS or CII stimulation for 20 h (fold change >2; $P < 0.05$). $n = 6$. (C) Venn diagram of differentially up-regulated genes after LPS or CII stimulation for 20 h in human MoDCs. $n = 6$. (D) Heatmap and clustering analysis of differentially up-regulated genes after LPS or CII stimulation for 20 h in human MoDCs. $n = 6$. (E) Bar plots of gene ontology analysis of the up-regulated genes in different clusters of (D). $n = 6$. (F) Gene tree analysis based on gene expression levels after LPS or CII stimulation for 20 h in human MoDCs. $n = 6$. (G, H) GSEA enrichment scores for indicated gene sets in CII (G) or LPS (H) stimulated human MoDCs. $n = 6$. (I) Transwell analysis of CCL19/21-triggered migration of BMDCs upon LPS (50 ng/mL) or CII (100 μg/mL) treatment for 20 h. $n = 3$. Data are presented as mean ± SD; ***$P < 0.001$.

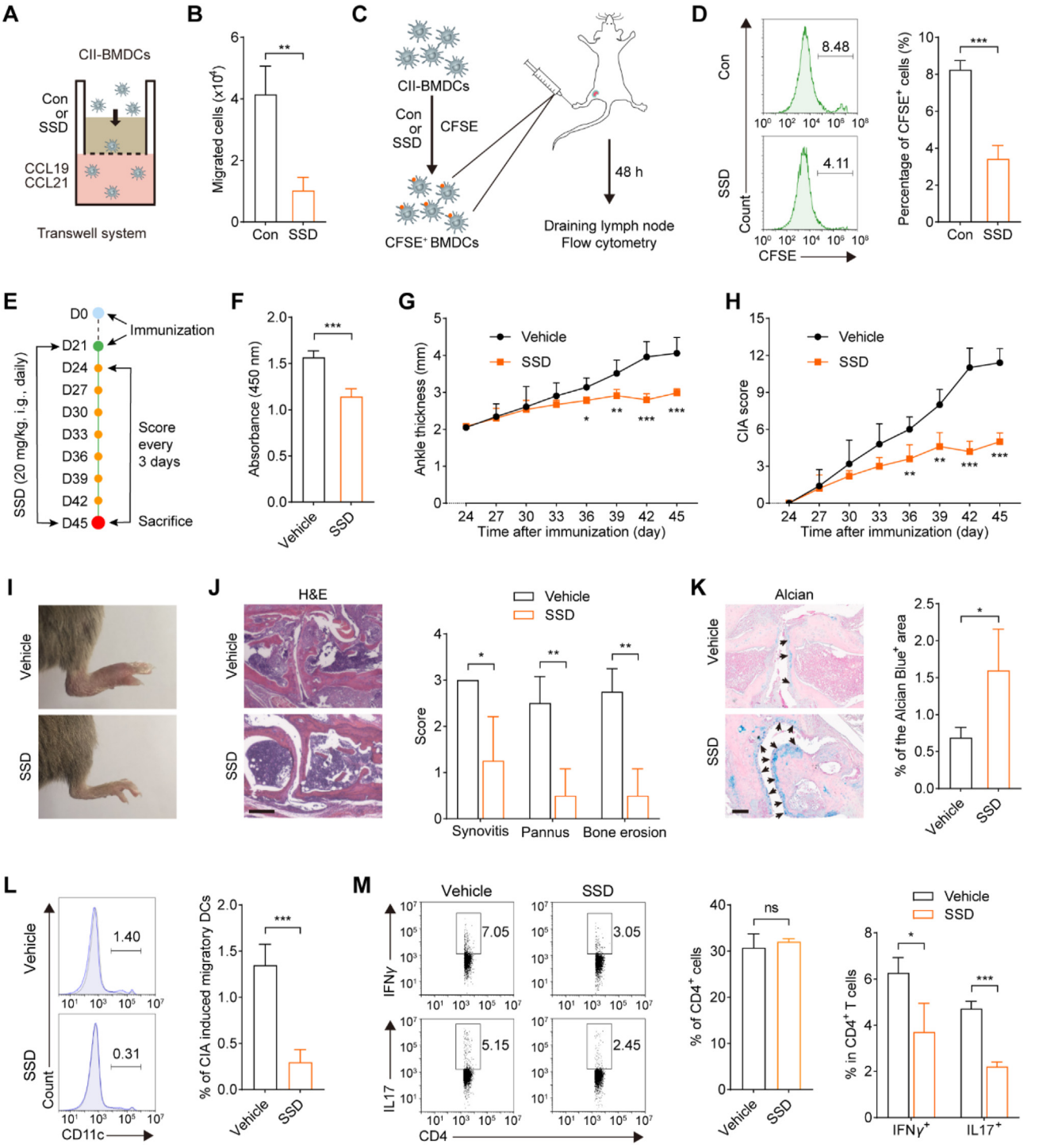

Figure 2 SSD impairs CII guided DC migration and alleviates CIA. (A) Scheme for Transwell analysis of chemokines-triggered migration of BMDCs after treating with CII (100 μg/mL) or SSD (1 μmol/L) for 24 h. (B) Quantification of migrated cells in (A). $n = 3$. (C) Scheme for *in vivo* migration of BMDCs with labeled CFSE after treating with CII (100 μg/mL) or SSD (1 μmol/L) for 24 h. (D) Representative images (left) and bar graph (right) for flow cytometry analysis of the migrated $CFSE^+$ BMDCs in (C). $n = 3$. (E) Scheme for the induction, assessment and administering of CIA mice. (F) Elisa of CII-specific IgG in the serum of vehicle or SSD treated CIA mice at 45 days post immunization (dpi 45). $n = 4$. (G, H) Ankle thickness (G) and CIA score (H) of vehicle or SSD treated CIA mice. $n = 5$ (* indicates a statistically difference when compared with vehicle group). (I) Representative images of paw swelling from vehicle or SSD treated CIA mice on dpi 45. (J) Representative images (left) and statistics (right) of H&E staining for paw sections from vehicle or SSD treated CIA mice on dpi 45. Scale bar: 100 μm. $n = 4$. (K) Representative images (left) and statistics (right) of Alcian Blue & Nuclear Fast Red staining for paw sections from vehicle or SSD treated CIA mice on dpi 45. Scale bar: 100 μm. $n = 4$. (L) Representative images (left) and bar graph (right) for flow cytometry analysis of the frequency of CIA-induced migratory $CD11c^+$ DCs (% in vehicle or SSD treated CIA mice−% in control mice) in the draining lymph node (DLN) of vehicle

3.3. SSD treatment alleviates the development of arthritis in CIA mouse model

Encouraged by the above findings, the collagen-induced arthritis (CIA) mouse model, the most commonly studied autoimmune model of rheumatoid arthritis, was then applied to evaluate the protective role of SSD on rheumatoid arthritis (Fig. 2E). The induction of CIA is critically dependent on immunization with CII, and the onset of arthritis is preceded by an early rise in CII-specific IgG autoantibodies[49,50], which was lessened in the CIA mice after SSD treatment (Fig. 2F). As expected, the clinical signs of arthritis, including ankle thickness, erythema, and swelling of every paw, developed on Day 24 after the first immunization and continuously progressed to Day 45, and SSD administration (20 mg/kg/day) resulted in a significant reduction of the ankle thickness and arthritic score (Fig. 2G and H). In addition, paw imaging and hematoxylin and eosin (H&E) staining revealed that paw swelling, synovial inflammatory infiltration, pannus formation, and bone erosion were powerfully suppressed in the joints of SSD-treated CIA mice (Fig. 2I and J). Consistently, Alcian Blue & Nuclear Fast Red staining also indicated SSD-treated CIA mice exhibited more intact cartilage in the damaged joints than vehicle-treated mice (Fig. 2K), indicating the protective role of SSD in the CIA mouse model.

Then, we analyzed the alteration of DC functions, including DC maturation and migration, in SSD-treated CIA mice. Flow cytometry results showed that the percentage of mature DCs marked with $CD80^+CD11c^+$ or $CD86^+CD11c^+$ antibodies was similar in DLNs from vehicle and SSD-treated CIA mice (Supporting Information Fig. S3A), consistent with our *in vitro* data that SSD did not affect the proportion of $CD80^+CD11c^+$ or $MHC\text{-}II^+CD11c^+$ mature DCs and cytokine expression upon CII stimulation in BMDCs (Fig. S3B and S3C). However, the percentage of CIA-induced migratory DCs in total DLN cells decreased remarkably after SSD treatment (Fig. 2L), suggesting an important role of SSD during DC migration rather than DC maturation in CIA mice. Given that the defects in DC migration interfere with the following antigen presentation and T cell activation and differentiation *in vivo*[4,23,51-53], the alteration of T cells was further examined in CIA mice by flow cytometry. Results showed that although SSD didn't affect the proportion of $CD4^+$ T cells in total DLN cells, SSD reduced the differentiation of pro-inflammatory Th1 ($CD4^+IFN\gamma^+$) and Th17 ($CD4^+IL17^+$) cells observably in DLNs (Fig. 2M). Overall, these results illustrate that SSD resists arthritis development in CIA mice, which may be related to SSD-suppressed DC migration.

3.4. OPTN is a potential target of SSD in CII-stimulated migratory DCs

We then investigated the underlying mechanism that SSD inhibited CII-mediated DC migration and arthritis alleviation. 1806 RA-associated regulators, which were extracted according to the relevance scores from the GeneCards database, were overlapped with 195 potential pharmacological targets of SSD, which were predicted from SwissTargetPrediction, STITCH, HERB, PharmMapper and Pubmed databases (Fig. 3A)[54]. Gene ontology (GO) analysis revealed most of the overlapped targets were enriched into positive regulation of cell migration, protein transport, regulation of apoptotic process, protein phosphorylation, and cytokine production (Fig. 3B). We then examined the expression of these targets in CII-stimulated DCs and found that among the upregulated candidates in CII-pulsed human monocyte-derived dendritic cells (moDCs), only the expression of OPTN, a well-recognized trafficking protein and autophagy receptor[25,26], could be significantly decreased by SSD (Fig. 3C−E). Further, Transwell assay combined with crystal violet staining results showed that OPTN overexpression in DC2.4 significantly accelerated SSD-suppressed cell migration (Fig. 3E and F), indicating that OPTN is a potential target of SSD during DC migration.

3.5. OPTN is required for CII-induced DC migration

To investigate whether OPTN regulates DC migration, *Optn* knockout (*Optn* KO) mice were applied (Fig. 4A). BMDCs from wildtype (WT) or *Optn* KO mice were isolated and cultured for DC migration assays *in vitro* and *in vivo*, and results showed that the migration of CII-stimulated *Optn* deficient BMDCs was blocked signally when compared to the control (Fig. 4B and C).

Then, CII-pulsed WT and *Optn* KO BMDCs were submitted for transcriptome profiling. A clear separation between WT and *Optn* KO BMDCs was observed by principal components analysis (PCA), and a set of differentially expressed genes (fold change >1.5, $P < 0.05$) were extracted for further analysis (Fig. 4D and E). GSEA manifested that genes significantly downregulated in *Optn* KO BMDCs were enriched in gene signatures associated with pseudopodia chemotaxis, extracellular matrix (ECM) structural constituent, focal adhesion assembly, and cytoskeletal trafficking, which were all related to chemokine receptors-mediated DC migration (Fig. 4F). On the contrary, gene signatures of the proteasome core complex were enriched in *Optn* KO BMDCs (Fig. 4F). Heatmap and qRT-PCR analysis further confirmed the expression of chemotaxis-related genes (*Ccl8*, *Akap12*), ECM genes (*Col1a2*, *Bgn*), cytoskeleton genes (*Myo3b*, *Rock1*), and adhesion-related genes (*Mmp9*, *Aebp1*) were reduced in CII-pulsed *Optn* deficient BMDCs compared with WT BMDCs (Fig. 4G and H).

Besides, it is widely recognized that the accumulation of the actin cytoskeleton, which shifts from a dispersed distribution, is crucial for facilitating DC migration. This process is characterized by the extension of pseudopods and alteration in cell stiffness, adhesion, and digestion properties[4]. In our study, immunofluorescence assays showed that F-actin, typically polymerized on one side in response to CII challenge, was instead evenly distributed around CII-pulsed *Optn* deficient BMDCs (Fig. 4I). This finding indicates that the absence of OPTN impairs CII-induced F-actin polarization to one side in DCs[45]. In summary, our results reinforce the notion that OPTN is indispensable for CII-mediated DC migration.

3.6. OPTN regulates CCR7 expression in CII-induced DC migration

We next sought to define the underlying mechanism whereby OPTN regulated CII-induced DC migration. The activation of DC chemokine receptors, like CCR7, CCR2, and CXCR4, induces an array of inside-out signals associated with chemotaxis, extracellular matrix regulation, cytoskeleton rearrangement, adhesion

or SSD treated CIA mice on dpi 45. $n = 4$. (M) Representative images (left) and bar graph (middle, right) for flow cytometry analysis of the frequency of $CD4^+$ T cells, Th1 ($CD4^+IFN\gamma^+$) and Th17 ($CD4^+IL17^+$) cells in the DLN of vehicle or SSD treated CIA mice on dpi 45. $n = 4$. Data are presented as mean ± SD; $^*P < 0.05$; $^{**}P < 0.01$; $^{***}P < 0.001$; ns, not significant.

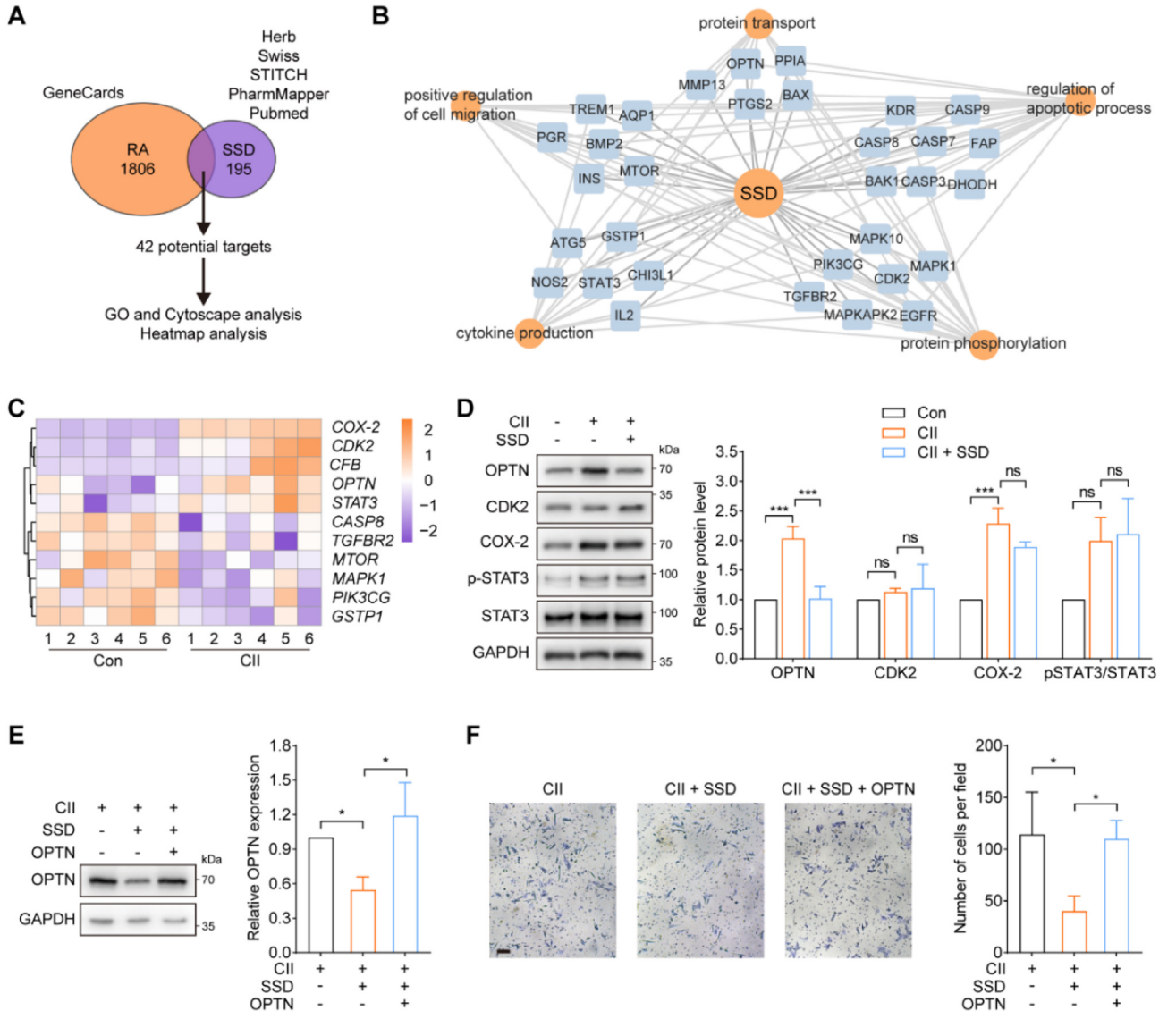

Figure 3 OPTN may be a potential target of SSD in CII-treated DCs. (A) Venn diagram analysis of the filtered RA-associated proteins and SSD potential targets from multiple databases. (B) GO analysis of the 42 potential targets screened in (A). (C) Heatmap analysis of the differentially expressed targets after CII stimulation for 20 h in human MoDCs. $n = 6$. (D) Western blotting (left) and quantification (right) analysis for the expression of OPTN, CDK2, COX-2, p-STAT3 and STAT3 in BMDCs after the treatment of CII (100 μg/mL) or SSD (1 μmol/L) for 24 h. $n = 3$. (E) Western blotting (left) and quantification (right) analysis for the expression of OPTN in DC2.4 after the transfection with OPTN plasmid and treating with CII (100 μg/mL) or SSD (1 μmol/L) for 24 h. $n = 3$. (F) Representative images (left) and statistics (right) for Transwell analysis together with crystal violet staining in DC2.4 after the transfection with OPTN plasmid and treating with CII (100 μg/mL) or SSD (1 μmol/L) for 24 h. Scale bar: 100 μm. $n = 3$. Data are presented as mean ± SD; $^*P < 0.05$; $^{***}P < 0.001$; ns, not significant.

property transformation, and metabolic energy activities, thus leading to DC migration[4,5,12]. Results showed that only CCR7 expression in BMDCs was notably elevated after CII stimulation and then inhibited upon *Optn* deficiency (Fig. 5A). Besides, flow cytometry results demonstrated the raised expression of membrane CCR7 upon CII stimulation was dramatically decreased in *Optn* KO BMDCs (Fig. 5B). Then, CCR7 was overexpressed to promote DC2.4 migration, while *Optn* knockdown significantly inhibited CCR7 expression and blocked cell migration (Fig. 5C and D). On the contrary, OPTN overexpression in DC2.4 upregulated the reduced expression of CCR7 caused by SSD treatment (Fig. 5E), indicating the positive regulation of OPTN on CCR7 expression in migrated DCs.

3.7. OPTN restrains the ubiquitin-proteasome degradation of CCR7 in DCs

Protein homeostasis is orchestrated by the balance between protein synthesis and degradation[55,56]. After treatment of cycloheximide (CHX), a reagent that was applied to block the *de novo* protein synthesis, *Optn* deficient BMDCs displayed lower expression and a shorter half-life of CCR7 protein without altering the mRNA level of *Ccr7* (Fig. 5F and G), revealing the potential role of OPTN in maintaining CCR7 homeostasis by inhibiting CCR7 protein degradation. Given that proteins are mainly degraded in ubiquitin-associated proteasome or autophagy-related lysosome, a proteasome inhibitor MG-132 and

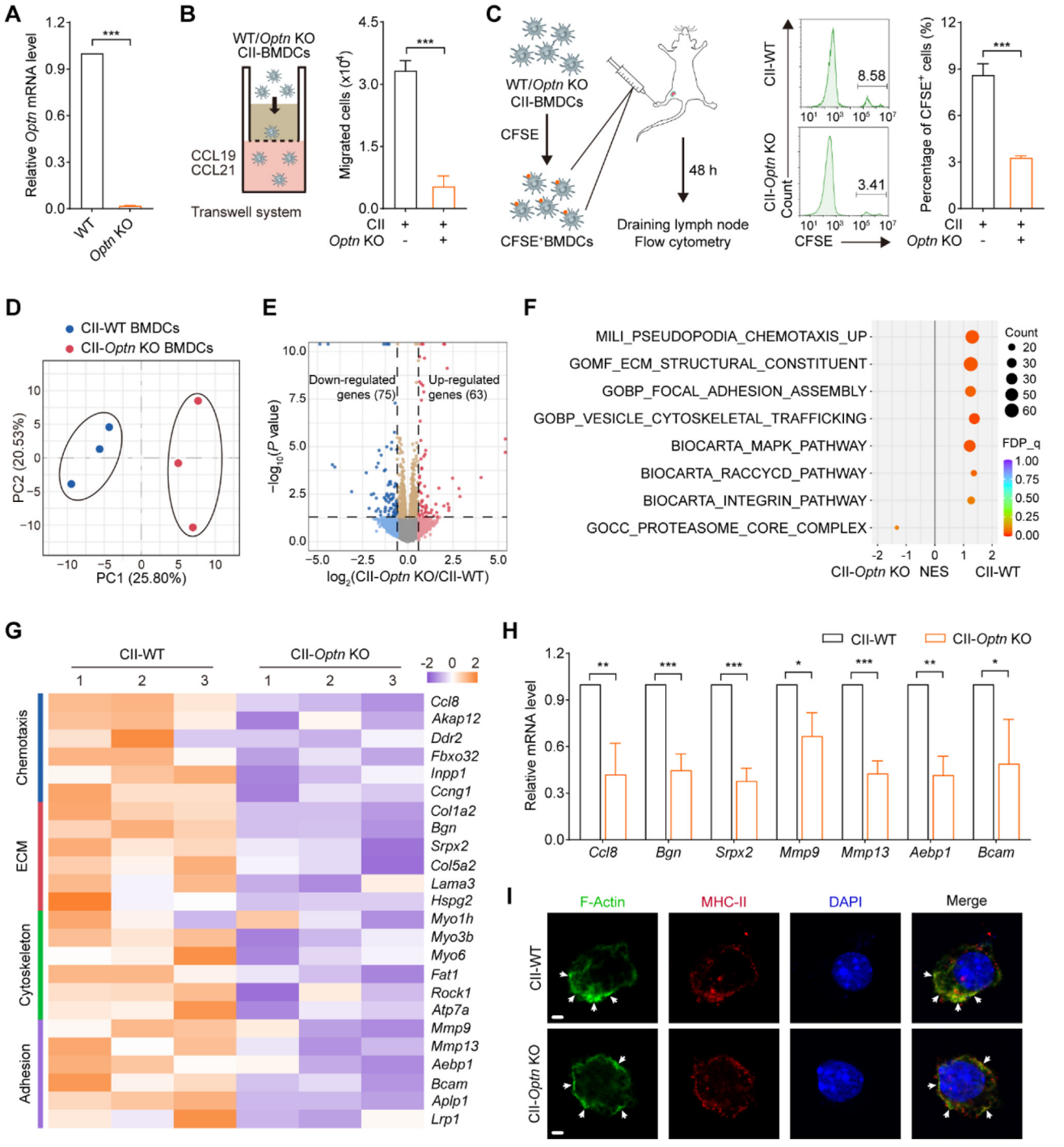

Figure 4 *Optn* deficiency hinders CII-induced DC migration. (A) qRT-PCR analyses of *Optn* in WT and *Optn* KO BMDCs. $n = 3$. (B) Scheme (left) and quantification (right) for Transwell analysis of CCL19/21-triggered migration of WT and *Optn* KO BMDCs after treating with CII (100 μg/mL) for 24 h. $n = 3$. (C) Scheme (left), representative images (middle) and bar graph (right) for the *in vivo* WT and *Optn* KO BMDC migration after labeling with CFSE and treating with CII (100 μg/mL) for 24 h. $n = 3$. (D) PCA analysis of transcriptome profiles of WT and *Optn* KO BMDCs after treating with CII (100 μg/mL) for 24 h. $n = 3$. (E) Volcano plot of transcriptome profiles of WT and *Optn* KO BMDCs after treating with CII (100 μg/mL) for 24 h ($P < 0.05$, fold-change >1.5). $n = 3$. (F) GSEA analyses of genes enriched in CII-pulsed WT or *Optn* KO BMDCs. $n = 3$. (G) Heatmap analyses of representative genes involved in cell migration in CII-pulsed WT or *Optn* KO BMDCs. $n = 3$. (H) qRT-PCR analyses of indicated genes in WT and *Optn* KO BMDCs after CII (100 μg/mL) treated for 24 h. $n = 3$. (I) Immunostaining of F-Actin (green) and membrane MHC-II (red) in WT and *Optn* KO BMDCs after CII (100 μg/mL) treatment for 24 h. Scale bar: 3 μm. $n = 3$. Data are presented as mean ± SD; $^*P < 0.05$; $^{**}P < 0.01$; $^{***}P < 0.001$.

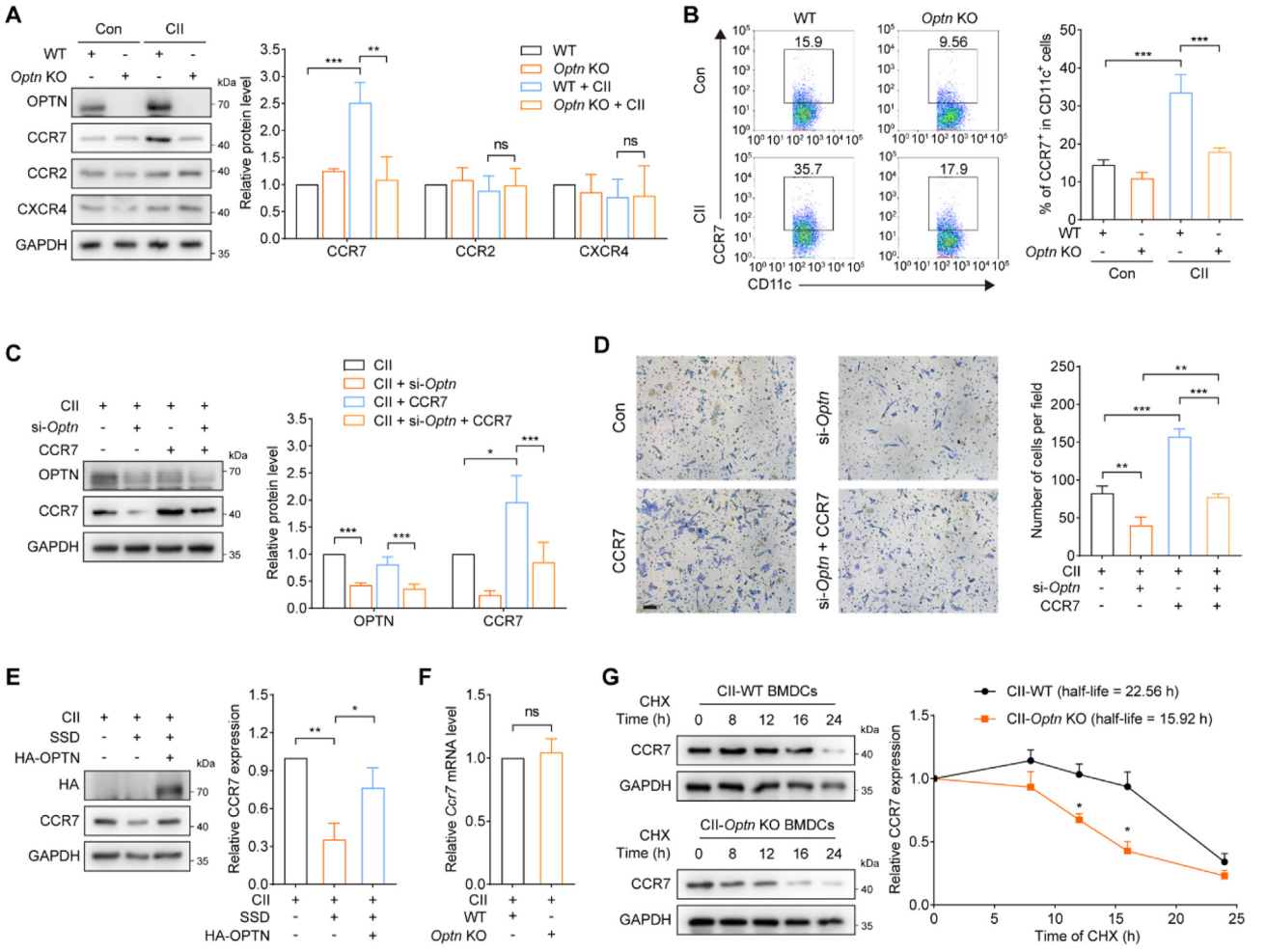

Figure 5 OPTN maintains CCR7 protein homeostasis in CII treated DCs. (A) Western blotting (left) and quantification (right) analysis for the expression of OPTN, CCR7, CCR2 and CXCR4 in WT and *Optn* KO BMDCs after the treatment with CII (100 μg/mL) for 24 h. $n = 3$. (B) Representative images (left) and bar graph (right) for flow cytometry analysis of the membrane protein expression of CCR7 in WT and *Optn* KO BMDCs after the treatment with CII (100 μg/mL) for 24 h. $n = 3$. (C) Western blotting (left) and quantification (right) analysis for the expression of OPTN and CCR7 in DC2.4 after the transfection with si-*Optn* or CCR7 plasmids and treating with CII (100 μg/mL) for 24 h. $n = 3$. (D) Representative images (left) and statistics (right) for Transwell analysis together with crystal violet staining in DC2.4 after the transfection with si-*Optn* or CCR7 plasmids and treating with CII (100 μg/mL) for 24 h. Scale bar: 100 μm. $n = 3$. (E) Western blotting (left) and quantification (right) analysis for the expression of HA and CCR7 in DC2.4 after the transfection with HA-OPTN plasmid and treating with CII (100 μg/mL) or SSD (1 μmol/L) for 24 h. $n = 3$. (F) qRT-PCR analysis of *Ccr7* genes in WT and *Optn* KO BMDCs after the treatment with CII (100 μg/mL) for 24 h. $n = 3$. (G) Western blotting (left) and quantification (right) analysis for the expression and half-life of CCR7 in WT and *Optn* KO BMDCs after the treatment with CHX (20 μg/mL) for different hours and CII (100 μg/mL) for 24 h. $n = 3$ (* indicates a statistically difference when compared with CII-WT group). Data are presented as mean ± SD; $^*P < 0.05$; $^{**}P < 0.01$; $^{***}P < 0.001$; ns, not significant.

a lysosome inhibitor chloroquine (CQ) were used to investigate how OPTN inhibited CCR7 degradation[55]. Western blotting results showed that it was MG-132 rather than CQ obviously inhibited the degradation of CCR7 and enhanced the migratory ability in *Optn* KO BMDCs (Fig. 6A and B). Therefore, these data indicated OPTN-regulated CCR7 degradation mainly occurred in proteasomes.

Previous studies showed that CCR7 is ubiquitylated in a constitutive, ligand-independent manner. Although its lysineless mutant can be properly inserted into the plasma membrane, ubiquitin-defective CCR7-7K7R was found to affect the transport and membrane recycling of CCR7[57]. Here, by co-immunoprecipitation analysis, we found that the ubiquitination of exogenous CCR7 was reduced upon OPTN overexpression in DC2.4 cells (Fig. 6C). Conversely, the ubiquitination of endogenous CCR7 was elevated in *Optn* KO BMDCs (Fig. 6D), and the co-localization of CCR7, ubiquitin, and 20S proteasome was increased in *Optn*-knockdown DC2.4 cells after proteasome inhibition (Fig. 6E and F). Altogether, these data further confirmed the ubiquitin-proteasome-dependent degradation of CCR7 restrained by OPTN.

Similarly, MG-132 increased the reduced CCR7 expression and the co-localization of CCR7 and 20S proteasome in SSD-treated DCs (Fig. 6G and H), indicating the proteasomal degradation of CCR7 caused by SSD in DCs. As expected, MG-132 notably increased the reduced number of migrated BMDCs after SSD treatment (Fig. 6I), suggesting the proteasomal

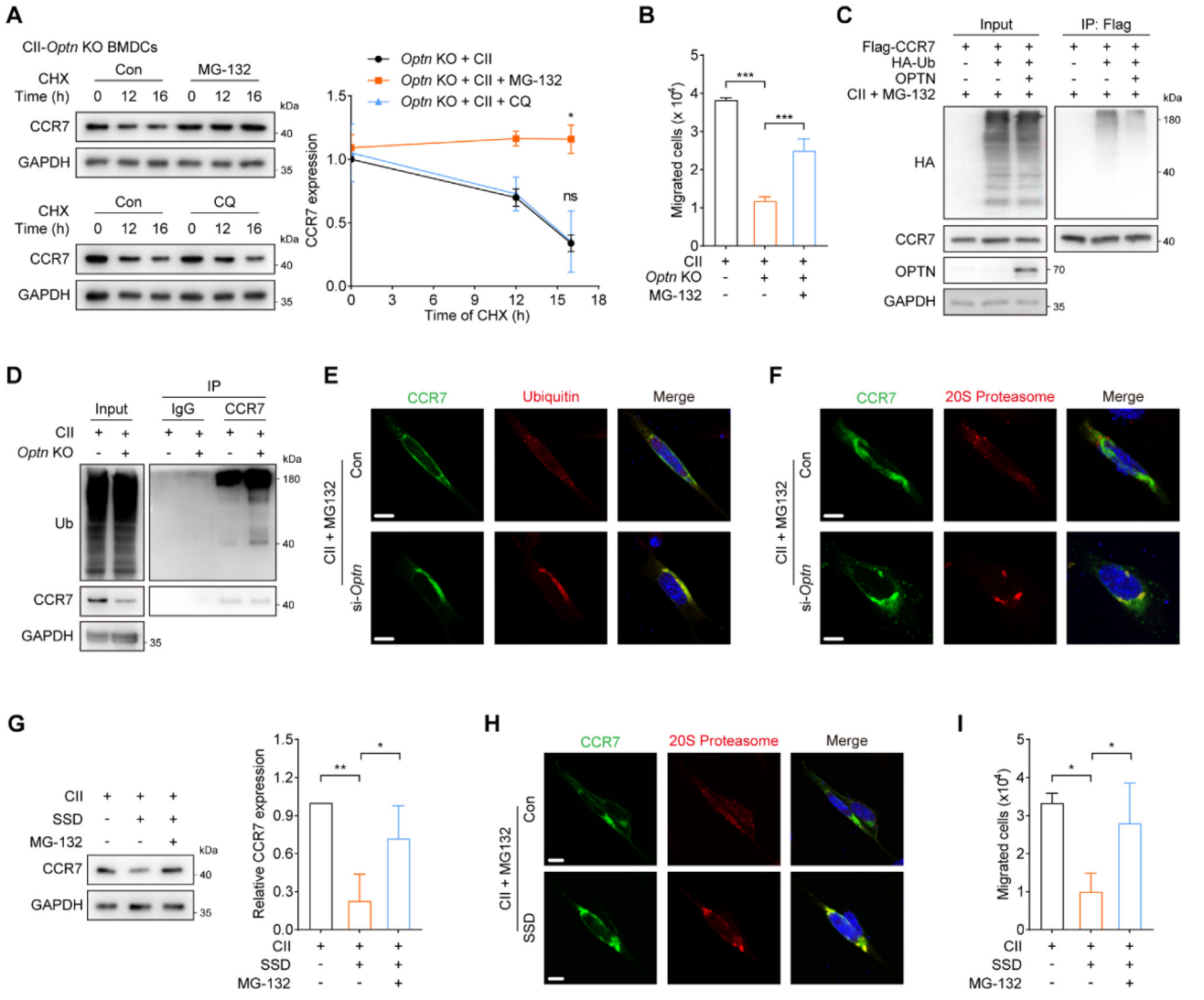

Figure 6 OPTN restrains the proteasome sorting and ubiquitin degradation of CCR7. (A) Western blotting (left) and quantification (right) analysis for the expression of CCR7 in *Optn* KO BMDCs after the treatment with CII (100 μg/mL) for 24 h, MG-132 (10 μmol/L) or CQ (10 μmol/L) for 12 h and CHX (20 μg/mL) for indicated times. $n = 3$ (* indicates a statistically difference when compared with *Optn* KO + CII group). (B) Transwell analysis of chemokines-triggered migration of WT or *Optn* KO BMDCs after treating with CII (100 μg/mL) for 24 h or MG-132 (10 μmol/L) for 12 h. $n = 3$. (C) Western blotting analysis for the ubiquitination (HA) of CCR7 by immunoprecipitation with Flag in DC2.4 after the transfection with Flag-CCR7, HA-Ub and OPTN plasmids and treating with CII (100 μg/mL) for 24 h, MG-132 (10 μmol/L) for 12 h. $n = 3$. (D) Western blotting analysis for endogenous ubiquitination of CCR7 by immunoprecipitation with CCR7 antibody in WT and *Optn* KO BMDCs after the treatment with CII (100 μg/mL) for 24 h. $n = 3$. (E) Immunostaining of CCR7 (green) and ubiquitin (red) in DC2.4 after the transfection with si-*Optn* plasmid and treating with CII (100 μg/mL) for 24 h, MG-132 (10 μmol/L) for 12 h. Scale bar: 10 μm. $n = 3$. (F) Immunostaining of CCR7 (green) and 20S proteasome α2 (red) in DC2.4 after the transfection with si-*Optn* plasmid and treating with CII (100 μg/mL) for 24 h, MG-132 (10 μmol/L) for 12 h. Scale bar: 10 μm. $n = 3$. (G) Western blotting (left) and quantification (right) analysis for the expression of CCR7 in BMDCs after the treatment with CII (100 μg/mL) for 24 h, SSD (1 μmol/L) for 24 h or MG-132 (10 μmol/L) for 12 h. $n = 3$. (H) Immunostaining of CCR7 (green) and 20S Proteasome α2 (red) in DC2.4 after the treatment with CII (100 μg/mL) for 24 h, MG-132 (10 μmol/L) for 12 h or SSD (1 μmol/L) for 24 h. Scale bar: 10 μm. $n = 3$. (I) Transwell analysis of chemokines-triggered migration of BMDCs after treating with CII (100 μg/mL) for 24 h, SSD (1 μmol/L) for 24 h or MG-132 (10 μmol/L) for 12 h $n = 3$. Data are presented as mean ± SD; $^*P < 0.05$; $^{**}P < 0.01$; $^{***}P < 0.001$; ns, not significant.

degradation of CCR7 is the key mechanism of SSD-regulated DC migration.

3.8. *Mice lacking Optn are refractory to the development of CIA*

Given the critical role of OPTN in CII-induced DC migration, we then generated *Optn* conditional knockout (*Optn* cKO) mice with conditional *Optn* ablation in CD11c$^+$ DCs by crossing *Optn*$^{flox/flox}$ mice with *CD11c*-Cre mice. WT and *Optn* cKO mice were immunized to employ the CIA model to explore the role of OPTN during RA progression (Fig. 7A). Expectedly, *Optn* cKO mice displayed milder CIA symptoms throughout the disease stages when compared with WT mice, as indicated by depressed CII-specific IgG levels in the serum, thinner swollen joints, and

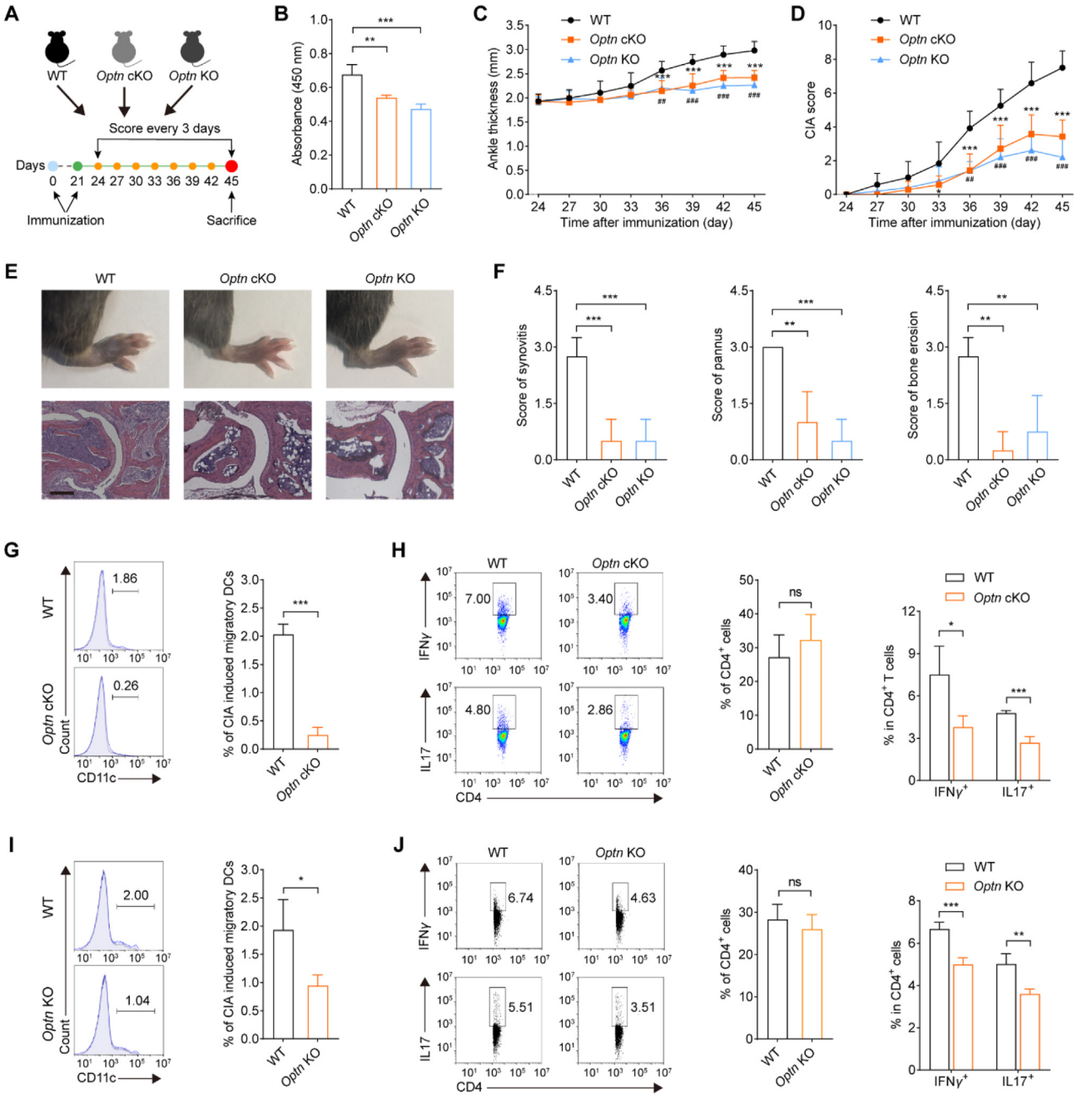

Figure 7 *Optn* deficiency impeded the progress of CIA. (A) Scheme for the induction and assessment of WT, *Optn* cKO and *Optn* KO CIA mice. (B) ELISA of CII-specific IgG in the serum of WT, *Optn* cKO and *Optn* KO CIA mice on dpi 45. $n = 4$. (C, D) Ankle thickness (C) and CIA score (D) in WT, *Optn* cKO and *Optn* KO CIA mice. $n = 12$ for WT, $n = 7$ for *Optn* cKO, $n = 5$ for *Optn* KO (* and $^{\#}$ indicate statistically difference when compared with WT group). (E) Representative images for paw swelling (above) and H&E staining of paw sections (bottom) from WT, *Optn* cKO and *Optn* KO CIA mice on dpi 45. (F) Statistics of synovitis, pannus and bone erosion of H&E staining in (E, bottom). $n = 4$. (G) Representative images (left) and bar graph (right) for flow cytometry analysis of the frequency of CIA-induced migratory $CD11c^+$ DCs (% in WT or *Optn* cKO CIA mice−% in control mice) in the DLN of WT and *Optn* cKO CIA mice on dpi 45. $n = 4$. (H) Representative images (left) and bar graph (middle, right) for flow cytometry analysis of the frequency of $CD4^+$ T cells, Th1 ($CD4^+IFN\gamma^+$) and Th17 ($CD4^+IL17^+$) cells in the DLN of WT and *Optn* cKO CIA mice on dpi 45. $n = 4$. (I) Representative images (left) and bar graph (right) for flow cytometry analysis of the frequency of CIA-induced migratory $CD11c^+$ DCs (% in WT or *Optn* KO CIA mice−% in control mice) in the DLN of WT and *Optn* KO CIA mice on dpi 45. $n = 4$. (J) Representative images (left) and bar graph (middle, right) for flow cytometry analysis of the frequency of $CD4^+$ T cells, Th1 ($CD4^+IFN\gamma^+$) and Th17 ($CD4^+IL17^+$) cells in the DLN of WT and *Optn* KO CIA mice on dpi 45. $n = 4$. Data are presented as mean ± SD; $^*P < 0.05$; $^{**}P < 0.01$; $^{***}P < 0.001$; $^{\#\#}P < 0.01$; $^{\#\#\#}P < 0.001$; ns, not significant.

lower clinical CIA scores (Fig. 7B−D). In addition, *Optn* cKO mice exhibited less damaged area in the affected joints (Fig. 7E and F). Then, the proportion of migratory DCs in total DLN cells was observably lower in *Optn* cKO mice (Fig. 7G), while a similar percentage of mature DCs was observed in *Optn* cKO DLNs and BMDCs (Fig. S3D−S3G). In consistence, the differentiation of pro-inflammatory $CD4^+IFN\gamma^+$ Th1 and $CD4^+IL17^+$ Th17 cells but not the percentage of $CD4^+$ T cells was also weaker prominently in these mice (Fig. 7H). Taken together, our findings represent a protective effect of *Optn* cKO on CIA, which may provide a great target for rheumatoid arthritis intervention.

Meanwhile, we also brought in *Optn* KO mice to generate the CIA model. Results showed that *Optn* KO mice presented alleviated CIA symptoms than WT mice (Fig. 7A−F, I and J). Besides, *Optn* KO did not influence DC maturation in either the CIA mouse model or CII-treated BMDCs (Fig. S3E−S3G). Interestingly, the CIA phenotype in *Optn* KO mice was similar to that in *Optn* cKO mice (Fig. 7B−F), suggesting that the predominant role of OPTN in the CIA model is to regulate DC migration, and targeting OPTN may be a potential strategy for rheumatoid arthritis therapy.

4. Discussion

DCs, as pivotal modulators of immune tolerance, are increasingly recognized as attractive targets for therapeutic strategies aimed at attenuating the immune response in RA. Upon antigen uptake, immature DCs in the synovium undergo maturation, during which they upregulate the expression of CCR7. Subsequently, the migration of DCs, facilitated by the CCL19/21−CCR7 axis, is a critical step that initiates T cell activation, ultimately leading to synovial inflammation and joint damage[4,5,51]. Thus, treatment with tolerogenic DCs or CCR7 antibody have been shown to restrain DC migration in arthritic mice and simultaneously reduce the severity and progression of RA[7,41]. Nevertheless, accumulating evidence indicates that signaling pathways induced by different antigens for DC activation are not uniform, and the use of appropriate antigens *in vitro* aid in identifying reliable disease targets[7,21-23]. Despite these advances, the pivotal molecules that mediate disease-specific DC activation in RA remain to be fully elucidated. In this study, by comparing the gene expression profiles of DCs stimulated by different antigens, we observed that RA-associated antigen CII significantly enhances DC migration compared to LPS (Fig. 1), underscoring the potential of targeting DC migration as a preventive strategy for RA.

Interestingly, SSD was identified here as an inhibitor to CII-specific DC migration, which then ameliorated CIA severity and reduced DC aggregation in DLN, suggesting its potential as a therapeutic agent for RA (Fig. 2). A recent study has also reported that SSD alleviates inflammation and regulates autophagy by inhibiting the PI3K/AKT/mTOR pathway, highlighting its potential as a therapeutic drug for osteoarthritis[38]. In addition, SSD has been found to obstruct the migration of hepatic stellate cells and endometrial cancer cells, thus controlling liver fibrosis and tumor progression, respectively[58,59]. However, another study indicates that SSD markedly increases the random migration of resident peritoneal macrophages, which may be associated with the disparate regulatory effects of SSD under different conditions[60].

Through a comprehensive database screening process, numerous potential targets were identified for SSD. In our previous research, we found SSD inhibits OPTN expression by binding to it and disrupting its stability[31]. Consistently, SSD was also found to suppress OPTN expression in CII-treated DCs, further confirming OPTN as a primary target of SSD in DCs (Fig. 3). Previous studies have shown that metformin significantly downregulates OPTN and then impedes the migration of ocular melanoma cells, underscoring the importance of OPTN in cell migration[61]. Nevertheless, a more in-depth investigation is required to elucidate other targets involved in SSD-regulated DC migration. On the other hand, the absence of OPTN revitalizes NF-κB and RANKL pathways, leading to enhanced osteoclast differentiation in synovial fibroblasts, which suggests a potential protective role of OPTN in RA[32,62]. In contrast to this finding, we observed that *Optn* knockout significantly mitigated CIA, possibly due in part to the suppression of DC trafficking (Fig. 7). These data suggest that OPTN has cell type-specific functions in regulating RA. This way, we still have not yet excluded the role of synovial fibroblasts in our CIA mouse model. It is essential to further explore the function of OPTN in other cell types that take part in the progression of RA.

Studies have demonstrated that CII can bind to its receptor TARM1 and OSCAR, thereby activating DCs[22,23]. In contrast, LPS, as used in our previous study, primarily elicits inflammatory responses by stimulating the TLR4-Myd88 signaling, which then leads to the activation of the JAK2/STAT3 pathway[63,64]. Concurrently, BMDCs lacking *Tarm1* displayed a diminished response to CII but not LPS[23]. Therefore, it is plausible that various antigens may elicit distinct responses in DCs, although the underlying mechanisms are not yet fully understood. Our previous study demonstrated that *Optn* knockout impairs DC maturation upon LPS stimulation through JAK2−STAT3 pathway[31]. However, our current study showed *Optn* knockout does not affect DC maturation, cytokine production, or JAK2−STAT3 activation following CII treatment (Figs. S3, S4A and S4B), indicating the OPTN-JAK2/STAT3 axis is not implicated in the CII-induced DC maturation. Moreover, after excluding the influence of OPTN on LPS-induced DC maturation, our data indicated that *Optn* deficiency did not significantly alter the migration ratio of mature BMDCs following LPS treatment. In contrast, the migration of mature DC induced by CII was found to be reduced in *Optn*-deficient DCs (Fig. S4C−S4E). Overall, these data underscore the pivotal role of antigen-specific DC activation and the distinguished regulation of OPTN upon different antigen stimulation in DCs.

It is known that RA is characterized by synovial inflammation, and the presence of significant levels of CII and anti-collagen antibodies in the serum or synovial fluid of RA patients underscores the importance of CII antigens in RA process[65-67]. Moreover, mature DCs can further induce CII release, contributing to a positive feedback loop that exacerbates the condition[13,20]. Notably, a study reported that the concentration of Coll 2-1 (the alpha-helical region of CII) in the serum of RA patients averaged 172.30 ± 19.05 nmol/L[66]. And a concentration of 100 μg/mL, which is equivalent to 333.33 nmol/L, has been consistently used in our *in vitro* experiments. Given the importance of CII-related DC migration in RA, we found that OPTN deficiency significantly inhibits CII-stimulated DC migration and mitigates the progression of RA (Figs. 4 and 7). This underscores the relevance of the antigenic microenvironment for the enhanced detection of disease targets. *In vivo*, the migration of DCs in CIA-induced WT mice increased by 1.86% (from 3.20% in control mice to 5.06% in WT CIA mice), which is a substantial increase of over 58% relative to DCs in control mice. In contrast, the *Optn* cKO CIA mice showed a much more modest increase of 0.26% (from 3.20% in control mice to 3.46% in *Optn* cKO CIA mice), representing

only an 8% increase to control (Fig. 7G). Thus, considering the inherently low baseline density of DCs in DLNs, even a minor increase in their proportion can lead to a substantial amplification[4,23,51-53]. Notably, the presence of increased DCs in synovium is also crucial for RA progression, rendering the study of synovial DCs highly pertinent to our research. Accurately determining the CII concentration in patients' synovial fluid is essential for more precisely examining the specific impacts of CII stimuli *in vitro*. While assessing peripheral DC migration in this study holds value, investigating synovial DCs remains of significant importance.

Targeting the CCR7 pathway is recognized as an effective strategy for modulating DC migration. It is well established that the expression and function of CCR7 are tightly regulated by a combination of mechanisms, including transcriptional control, post-translational modifications, internalization, degradation, and recycling processes[4,5]. However, there is a scarcity of studies on the degradation specific to CCR7. The limited research available indicates that CCR7 has a long half-life and is constitutively ubiquitylated in a ligand-independent manner, a process crucial for its internalization and plasma membrane recycling[4,57]. Despite this, the specific E3 ubiquitin ligase responsible for CCR7 ubiquitination remains unidentified[57,68]. Consistently, we observed that the half-life of CCR7 was notably long. Interestingly, we found the absence of OPTN significantly reduced the half-life of CCR7 (Fig. 5), thereby impeding CCR7-mediated DC migration. Recently, Wan Du and colleagues demonstrated that OPTN can interact with AP3D1 to prevent the lysosomal sorting and degradation of palmitoylated IFNGR1, thereby maintaining the integrity of IFNγ signaling and enhancing the efficacy of immunotherapy[55]. In our study, we discovered that OPTN, as well as its inhibitor SSD, regulated the proteasomal sorting and ubiquitin-dependent degradation of CCR7 (Fig. 6), thus providing additional insight into the biological regulation of CCR7.

As a multifunctional autophagy regulator, OPTN promotes the ubiquitination, autolysosome fusion, and autophagy degradation of substrate protein[26,31]. In this study, we also investigated the role of OPTN in the autophagic regulation of DC migration. Upon CII stimulation, we observed a significant autophagy induction, indicated by an elevated LC3II/I ratio and an increase in autophagic flux after CII treatment (Supporting Information Fig. S5A−S5C), which may be a trigger for DC migration[69-71]. Then, the regulation of autophagy through pharmacological interventions effectively negated the impact of either OPTN deficiency or overexpression on CCR7 expression and CII-induced DC migration (Fig. S5D−S5G). These findings suggest that OPTN-mediated autophagy participates in CCR7 degradation and CCR7-mediated DC migration. Nevertheless, Co-IP assay results indicated there was no direct binding between OPTN and CCR7 protein (Fig. S5H), indicating that OPTN may not directly regulate CCR7 degradation. Considering that OPTN restrains the proteasomal sorting and ubiquitin-dependent degradation of CCR7 to promote DC migration (Figs. 5 and 6), we then propose a hypothesis that autophagy mediated by OPTN may induce the degradation of an intermediary protein, which is essential for the ubiquitin-dependent degradation of CCR7 in DC migration. It is plausible that the intermediary protein could be an E3 ubiquitin ligase specific to CCR7, which may be upregulated in the absence of OPTN and could facilitate the degradation of CCR7. Given the current limited understanding of the CCR7 degradation pathways and the associated E3 ligases, further research is essential to uncover the molecular events underlying the OPTN-regulated DC migration.

5. Conclusions

In summary, our study showed that the RA-specific antigen CII preferentially activates DC migration signaling pathways over those involved in DC maturation. We demonstrated that OPTN facilitates CII-induced DC migration by inducing autophagy and restraining CCR7 degradation. Conversely, the reduction of OPTN expression by SSD inhibits DC migration by allowing for increased CCR7 degradation, which effectively ameliorates the symptoms of RA (Supporting Information Fig. S6). Our findings not only highlight targeting DC migration as a novel and specific strategy for RA treatment, but also elucidate a new role for OPTN in regulating DC migration. Furthermore, we propose OPTN as a promising therapeutic target and suggest the potential for DC-based immunotherapy in the management of RA.

Data availability

The microarray gene chip data of human MoDCs stimulated by LPS or CII were downloaded from the EMBL-EBI ArrayExpress depository (accession no. E-MTAB-2904). The RNA-seq data of CII-challenged WT or *Optn* KO BMDCs were deposited in the NCBI Gene Expression Omnibus database (accession No. GSE 240706).

Acknowledgments

We thank Prof. Ronggui Hu for the gifts of *Optn* KO and *Optn*$^{flox/flox}$ mice, thank Prof. Ronggui Hu and Prof. Hong Zhu for the gifts of plasmids, thank Prof. Zhen Gu for the gifts of DC2.4. We acknowledge the financial support by the National Natural Science Foundation of China (Nos. 82222069, 82273935, 82104177, 82073857 and 81872878), the Key R&D Program of Zhejiang (No. 2022C03077, China), the Fundamental Research Funds for the Central Universities (No. 226-2024-00094, China), and the Opening Fund of Key Laboratory of Drug Safety Evaluation and Research of Zhejiang Province.

Author contributions

Wenxiang Hong: Writing − original draft, Methodology, Investigation, Formal analysis, Data curation, Conceptualization. Hongbo Ma: Methodology, Investigation, Data curation. Zhaoxu Yang: Methodology, Formal analysis, Data curation. Jiaying Wang: Resources, Funding acquisition, Conceptualization. Bowen Peng: Investigation, Data curation. Longling Wang: Methodology, Investigation, Data curation. Yiwen Du: Methodology, Investigation, Data curation. Lijun Yang: Validation, Funding acquisition, Data curation. Lijiang Zhang: Validation, Funding acquisition. Zhibin Li: Methodology, Investigation, Data curation. Han Huang: Methodology, Investigation, Data curation. Difeng Zhu: Methodology, Investigation. Bo Yang: Writing − review & editing, Validation, Supervision. Qiaojun He: Writing − review & editing, Validation, Supervision. Jiajia Wang: Writing − review & editing, Validation, Supervision, Resources, Funding acquisition, Conceptualization. Qinjie Weng: Writing − review & editing, Validation, Supervision, Resources, Project administration, Funding acquisition, Conceptualization.

Conflicts of interest

The authors declare that they have no conflict of interest.

Appendix A. Supporting information

Supporting information to this article can be found online at https://doi.org/10.1016/j.apsb.2025.02.004.

References

1. Itai YS, Barboy O, Salomon R, Bercovich A, Xie K, Winter E, et al. Bispecific dendritic-T cell engager potentiates anti-tumor immunity. *Cell* 2024;**187**:375−89.e18.
2. Hanc P, Gonzalez RJ, Mazo IB, Wang YD, Lambert T, Ortiz G, et al. Multimodal control of dendritic cell functions by nociceptors. *Science* 2023;**379**:eabm5658.
3. Pittet MJ, Di Pilato M, Garris C, Mempel TR. Dendritic cells as shepherds of T cell immunity in cancer. *Immunity* 2023;**56**:2218−30.
4. Hong W, Yang B, He Q, Wang J, Weng Q. New insights of CCR7 signaling in dendritic cell migration and inflammatory diseases. *Front Pharmacol* 2022;**13**:841687.
5. Liu J, Zhang XM, Cheng YJ, Cao XT. Dendritic cell migration in inflammation and immunity. *Cell Mol Immunol* 2021;**18**:2461−71.
6. Di Matteo A, Bathon JM, Emery P. Rheumatoid arthritis. *Lancet* 2023; **402**:2019−33.
7. Stoop JN, Harry RA, von Delwig A, Isaacs JD, Robinson JH, Hilkens CM. Therapeutic effect of tolerogenic dendritic cells in established collagen-induced arthritis is associated with a reduction in Th17 responses. *Arthritis Rheum* 2010;**62**:3656−65.
8. Weyand CM, Goronzy JJ. The immunology of rheumatoid arthritis. *Nat Immunol* 2021;**22**:10−8.
9. Guo PP, Jiang J, Chu R, He F, Ge ML, Fang RH, et al. GRK2 mediated degradation of SAV1 initiates hyperplasia of fibroblast-like synoviocytes in rheumatoid arthritis. *Acta Pharm Sin B* 2024;**14**:1222−40.
10. Xue M, Lin H, Liang HPH, Bereza-Malcolm L, Lynch T, Sinnathurai P, et al. EPCR deficiency ameliorates inflammatory arthritis in mice by suppressing the activation and migration of T cells and dendritic cells. *Rheumatol* 2024;**63**:571−80.
11. Woo MS, Ufer F, Sonner JK, Belkacemi A, Tintelnot J, Saez PJ, et al. Calcium channel beta3 subunit regulates ATP-dependent migration of dendritic cells. *Sci Adv* 2023;**9**:eadh1653.
12. Worbs T, Hammerschmidt SI, Forster R. Dendritic cell migration in health and disease. *Nat Rev Immunol* 2017;**17**:30−48.
13. Yu MB, Langridge WHR. The function of myeloid dendritic cells in rheumatoid arthritis. *Rheumatol Int* 2017;**37**:1043−51.
14. Cosway E, Anderson G, Garside P, Prendergast C. The thymus and rheumatology: should we care?. *Curr Opin Rheumatol* 2016;**28**: 189−95.
15. Bosnjak B, Do KTH, Forster R, Hammerschmidt SI. Imaging dendritic cell functions. *Immunol Rev* 2022;**306**:137−63.
16. Burkhardt H, Sehnert B, Bockermann R, Engstrom A, Kalden JR, Holmdahl R. Humoral immune response to citrullinated collagen type II determinants in early rheumatoid arthritis. *Eur J Immunol* 2005;**35**: 1643−52.
17. Jabbari M, Barati M, Khodaei M, Babashahi M, Kalhori A, Tahmassian AH, et al. Is collagen supplementation friend or foe in rheumatoid arthritis and osteoarthritis? A comprehensive systematic review. *Int J Rheum Dis* 2022;**25**:973−81.
18. Yang XZ, Zhao YJ, Wei Q, Zhu XM, Wang LP, Zhang WK, et al. GRK2 inhibits Flt-1D macrophage infiltration and its proangiogenic properties in rheumatoid arthritis. *Acta Pharm Sin B* 2024;**14**: 241−55.
19. Dodge GR, Poole AR. Immunohistochemical detection and immunochemical analysis of type II collagen degradation in human normal, rheumatoid, and osteoarthritic articular cartilages and in explants of bovine articular cartilage cultured with interleukin 1. *J Clin Investig* 1989;**83**:647−61.
20. Lakey RL, Morgan TG, Rowan AD, Isaacs JD, Cawston TE, Hilkens CM. A novel paradigm for dendritic cells as effectors of cartilage destruction. *Rheumatol* 2009;**48**:502−7.
21. Leung BP, Conacher M, Hunter D, McInnes IB, Liew FY, Brewer JM. A novel dendritic cell-induced model of erosive inflammatory arthritis: distinct roles for dendritic cells in T cell activation and induction of local inflammation. *J Immunol* 2002;**169**:7071−7.
22. Schultz HS, Nitze LM, Zeuthen LH, Keller P, Gruhler A, Pass J, et al. Collagen induces maturation of human monocyte-derived dendritic cells by signaling through osteoclast-associated receptor. *J Immunol* 2015;**194**:3169−79.
23. Yabe R, Chung SH, Murayama MA, Kubo S, Shimizu K, Akahori Y, et al. TARM1 contributes to development of arthritis by activating dendritic cells through recognition of collagens. *Nat Commun* 2021; **12**:94.
24. Jin J, Huang R, Chang Y, Yi X. Roles and mechanisms of optineurin in bone metabolism. *Biomed Pharmacother* 2024;**172**:116258.
25. Guo Q, Wang J, Weng Q. The diverse role of optineurin in pathogenesis of disease. *Biochem Pharmacol* 2020;**180**:114157.
26. Qiu Y, Wang J, Li H, Yang B, Wang J, He Q, et al. Emerging views of OPTN (optineurin) function in the autophagic process associated with disease. *Autophagy* 2022;**18**:73−85.
27. Byrnes K, Blessinger S, Bailey NT, Scaife R, Liu G, Khambu B. Therapeutic regulation of autophagy in hepatic metabolism. *Acta Pharm Sin B* 2022;**12**:33−49.
28. Yadav M, Bhardwaj A, Yadav A, Dada R, Tanwar M. Molecular genetics of primary open-angle glaucoma. *Indian J Ophthalmol* 2023;**71**: 1739−56.
29. Mou Y, Li M, Liu M, Wang J, Zhu G, Zha Y. OPTN variants in ALS cases: a case report of a novel mutation and literature review. *Neurol Sci* 2022;**43**:5391−6.
30. Sudhakar C, Vaibhava V, Swarup G. IRF-1-binding site in the first intron mediates interferon-γ-induced optineurin promoter activation. *Biochem Biophys Res Commun* 2013;**437**:179−84.
31. Wang J, Wang J, Hong W, Zhang L, Song L, Shi Q, et al. Optineurin modulates the maturation of dendritic cells to regulate autoimmunity through JAK2−STAT3 signaling. *Nat Commun* 2021;**12**:6198.
32. Lee WS, Kato M, Sugawara E, Kono M, Kudo Y, Kono M, et al. Protective role of optineurin against joint destruction in rheumatoid arthritis synovial fibroblasts. *Arthritis Rheumatol* 2020;**72**:1493−504.
33. Yuan J, Tao Y, Wang M, Huang F, Wu X. Natural compounds as potential therapeutic candidates for multiple sclerosis: emerging preclinical evidence. *Phytomedicine* 2024;**123**:155248.
34. Moudgil KD, Venkatesha SH. The anti-inflammatory and immunomodulatory activities of natural products to control autoimmune inflammation. *Int J Mol Sci* 2022;**24**:95.
35. Umbreen H, Zhang X, Tang KT, Lin CC. Regulation of myeloid dendritic cells by synthetic and natural compounds for the treatment of rheumatoid arthritis. *Int J Mol Sci* 2022;**24**:238.
36. Tang X, Wang CX, Wang L, Ren FF, Kuang RQ, Li ZH, et al. Aureane-type sesquiterpene tetraketides as a novel class of immunomodulators with interleukin-17A inhibitory activity. *Acta Pharm Sin B* 2023;**13**:3930−44.
37. Duan YL, Sun WG, Li YQ, Shi ZY, Li LQ, Zhang YT, et al. Spirohypertones A and B as potent antipsoriatics: tumor necrosis factor-α inhibitors with unprecedented chemical architectures. *Acta Pharm Sin B* 2024;**14**:2646−56.
38. Jiang J, Meng Y, Hu S, Botchway BOA, Zhang Y, Liu X. Saikosaponin D: a potential therapeutic drug for osteoarthritis. *J Tissue Eng Regen Med* 2020;**14**:1175−84.
39. Gao T, Wang T, Wu L, Tong Y, Tian J, Zhao K, et al. Saikosaponin-d alleviates depression by promoting NLRP3 ubiquitination and inhibiting inflammasome activation. *Int Immunopharmacol* 2024;**127**: 111324.
40. Chen S, Wang K, Wang H, Gao Y, Nie K, Jiang X, et al. The therapeutic effects of saikosaponins on depression through the modulation of neuroplasticity: from molecular mechanisms to potential clinical applications. *Pharmacol Res* 2024;**201**:107090.
41. Moschovakis GL, Bubke A, Friedrichsen M, Ristenpart J, Back JW, Falk CS, et al. The chemokine receptor CCR7 is a promising target for rheumatoid arthritis therapy. *Cell Mol Immunol* 2019;**16**:791−9.

42. Moulin D, Millard M, Taieb M, Michaudel C, Aucouturier A, Lefevre A, et al. Counteracting tryptophan metabolism alterations as a new therapeutic strategy for rheumatoid arthritis. *Ann Rheum Dis* 2024;**83**:312−23.
43. Lv CJ, Sun MH, Guo YL, Xia WX, Qiao SM, Tao Y, et al. Cholinergic dysfunction-induced insufficient activation of α7 nicotinic acetylcholine receptor drives the development of rheumatoid arthritis through promoting protein citrullination *via* the SP3/PAD4 pathway. *Acta Pharm Sin B* 2023;**13**:1600−15.
44. Wu G, Cao B, Zhai HG, Liu B, Huang Y, Chen XW, et al. EPO promotes the progression of rheumatoid arthritis by inducing desialylation *via* increasing the expression of neuraminidase 3. *Ann Rheum Dis* 2024;**83**:564−75.
45. Liu J, Zhang X, Chen K, Cheng Y, Liu S, Xia M, et al. CCR7 chemokine receptor-inducible lnc-Dpf3 restrains dendritic cell migration by inhibiting HIF-1α-mediated glycolysis. *Immunity* 2019;**50**:600−15.e15.
46. Ru J, Li P, Wang J, Zhou W, Li B, Huang C, et al. TCMSP: a database of systems pharmacology for drug discovery from herbal medicines. *J Cheminform* 2014;**6**:13.
47. Wu Y, Fang Y, Li Y, Au R, Cheng C, Li W, et al. A network pharmacology approach and experimental validation to investigate the anticancer mechanism of Qi-Qin-Hu-Chang formula against colitis-associated colorectal cancer through induction of apoptosis *via* JNK/p38 MAPK signaling pathway. *J Ethnopharmacol* 2024;**319**:117323.
48. Chen T, Lei Y, Li M, Liu X, Zhang L, Cai F, et al. Network pharmacology to unveil the mechanism of suanzaoren decoction in the treatment of Alzheimer's with diabetes. *Hereditas* 2024;**161**:2.
49. Wei Z, Kawashima H. Prevention of collagen-induced arthritis by an anti-glycan monoclonal antibody reactive with 6-sulfo sialyl Lewis x in DBA/1 mice. *Monoclon Antib Immunodiagn Immunother* 2024;**43**:3−9.
50. Stuart JM, Dixon FJ. Serum transfer of collagen-induced arthritis in mice. *J Exp Med* 1983;**158**:378−92.
51. Wang Z, Zhang J, An F, Zhang J, Meng X, Liu S, et al. The mechanism of dendritic cell-T cell crosstalk in rheumatoid arthritis. *Arthritis Res Ther* 2023;**25**:193.
52. Yamada S, Nagafuchi Y, Wang M, Ota M, Hatano H, Takeshima Y, et al. Immunomics analysis of rheumatoid arthritis identified precursor dendritic cells as a key cell subset of treatment resistance. *Ann Rheum Dis* 2023;**82**:809−19.
53. Hilkens CMU, Isaacs JD. Tolerogenic dendritic cell therapy for rheumatoid arthritis: where are we now?. *Clin Exp Immunol* 2013;**172**:148−57.
54. Zhou J, Zhang F, Chen J, Zhang S, Wang H. Chlorogenic acid inhibits human glioma U373 cell progression *via* regulating the SRC/MAPKs signal pathway: based on network pharmacology analysis. *Drug Des Devel Ther* 2021;**15**:1369−83.
55. Du W, Hua F, Li X, Zhang J, Li S, Wang W, et al. Loss of optineurin drives cancer immune evasion *via* palmitoylation-dependent IFNGR1 lysosomal sorting and degradation. *Cancer Discov* 2021;**11**:1826−43.
56. Huang XW, Wu FB, Ye J, Wang L, Wang XY, Li X, et al. Expanding the horizons of targeted protein degradation: a non-small molecule perspective. *Acta Pharm Sin B* 2024;**14**:2402−27.
57. Schaeuble K, Hauser MA, Rippl AV, Bruderer R, Otero C, Groettrup M, et al. Ubiquitylation of the chemokine receptor CCR7 enables efficient receptor recycling and cell migration. *J Cell Sci* 2012;**125**:4463−74.
58. Tang TT, Jiang L, Zhong Q, Ni ZJ, Thakur K, Khan MR, et al. Saikosaponin D exerts cytotoxicity on human endometrial cancer ishikawa cells by inducing apoptosis and inhibiting metastasis through MAPK pathways. *Food Chem Toxicol* 2023;**177**:113815.
59. Chen MF, Huang CC, Liu PS, Chen CH, Shiu LY. Saikosaponin a and saikosaponin d inhibit proliferation and migratory activity of rat HSC-T6 cells. *J Med Food* 2013;**16**:793−800.
60. Ushio Y, Abe H. The effects of saikosaponin on macrophage functions and lymphocyte proliferation. *Planta Med* 1991;**57**:511−4.
61. Zhuang A, Chai P, Wang S, Zuo S, Yu J, Jia S, et al. Metformin promotes histone deacetylation of optineurin and suppresses tumour growth through autophagy inhibition in ocular melanoma. *Clin Transl Med* 2022;**12**:e660.
62. Xue P, Hu X, Chang E, Wang L, Chen M, Wu TH, et al. Deficiency of optineurin enhances osteoclast differentiation by attenuating the NRF2-mediated antioxidant response. *Exp Mol Med* 2021;**53**:667−80.
63. Oh J, Kwon TW, Choi JH, Kim Y, Moon SK, Nah SY, et al. Ginsenoside-Re inhibits experimental autoimmune encephalomyelitis as a mouse model of multiple sclerosis by downregulating TLR4/MyD88/NF-κB signaling pathways. *Phytomedicine* 2024;**122**:155065.
64. Liu J, Kang R, Tang D. Lipopolysaccharide delivery systems in innate immunity. *Trends Immunol* 2024;**45**:274−87.
65. Prince HE. Biomarkers for diagnosing and monitoring autoimmune diseases. *Biomarkers* 2005;**10**:S44−9.
66. Deberg M, Labasse A, Christgau S, Cloos P, Henriksen DB, Chapelle JP, et al. New serum biochemical markers (Coll 2-1 and Coll 2-1 NO2) for studying oxidative-related type II collagen network degradation in patients with osteoarthritis and rheumatoid arthritis. *Osteoarthr Cartilage* 2005;**13**:258−65.
67. Batsalova T, Dzhambazov B. Significance of type II collagen post-translational modifications: from autoantigenesis to improved diagnosis and treatment of rheumatoid arthritis. *Int J Mol Sci* 2023;**24**:9884.
68. Otero C, Groettrup M, Legler DF. Opposite fate of endocytosed CCR7 and its ligands: recycling versus degradation. *J Immunol* 2006;**177**:2314−23.
69. Wildenberg ME, Koelink PJ, Diederen K, Te Velde AA, Wolfkamp SC, Nuij VJ, et al. The ATG16L1 risk allele associated with Crohn's disease results in a Rac1-dependent defect in dendritic cell migration that is corrected by thiopurines. *Mucosal Immunol* 2017;**10**:352−60.
70. Shen TP, Zhu WC, Yang L, Liu L, Jin RR, Duan JM, et al. Lactosylated *N*-alkyl polyethylenimine coated iron oxide nanoparticles induced autophagy in mouse dendritic cells. *Regen Biomater* 2018;**5**:141−9.
71. Khan N, Pahari S, Vidyarthi A, Aqdas M, Agrewala JN. NOD-2 and TLR-4 signaling reinforces the efficacy of dendritic cells and reduces the dose of TB drugs against *Mycobacterium tuberculosis*. *J Innate Immun* 2016;**8**:228−42.